

# **Three-Dimensional Property Modelling of the Upper Cretaceous Cardium Formation in West-Central and Southern Alberta**

**AER/AGS Open File Report 2020-01**

# **Three-Dimensional Property Modelling of the Upper Cretaceous Cardium Formation in West- Central and Southern Alberta**

S. Mei and M. Berhane

Alberta Energy Regulator  
Alberta Geological Survey

February 2020

©Her Majesty the Queen in Right of Alberta, 2020

ISBN 978-1-4601-4601-4505-0

The Alberta Energy Regulator / Alberta Geological Survey (AER/AGS), its employees and contractors make no warranty, guarantee or representation, express or implied, or assume any legal liability regarding the correctness, accuracy, completeness or reliability of this publication. Any references to proprietary software and/or any use of proprietary data formats do not constitute endorsement by AER/AGS of any manufacturer's product.

If you use information from this publication in other publications or presentations, please acknowledge the AER/AGS. We recommend the following reference format:

Mei, S. and Berhane, M. (2020): Three-dimensional property modelling of the Upper Cretaceous Cardium Formation in west-central and southern Alberta; Alberta Energy Regulator / Alberta Geological Survey, AER/AGS Open File Report 2020-01, 47 p.

Publications in this series have undergone only limited review and are released essentially as submitted by the author.

**Published February 2020 by:**

Alberta Energy Regulator  
Alberta Geological Survey  
4th Floor, Twin Atria Building  
4999 – 98th Avenue  
Edmonton, AB T6B 2X3  
Canada

Tel: 780.638.4491  
Fax: 780.422.1459  
Email: [AGS-Info@aer.ca](mailto:AGS-Info@aer.ca)  
Website: [www.ags.aer.ca](http://www.ags.aer.ca)

## Contents

Acknowledgements.....	vi
Abstract.....	vii
1 Introduction.....	1
1.1 Study Area .....	1
2 Stratigraphic Framework .....	3
3 Data and Compilation .....	5
4 Methods and Workflow .....	7
4.1 Log Analysis .....	7
4.1.1 Shale Volume Calculation .....	7
4.1.2 Density Log Processing .....	7
4.1.3 Density Porosity Calculation.....	7
4.1.4 Water Saturation Calculation.....	8
5 3D Modelling in Petrel .....	9
5.1 Input Source Data .....	9
5.2 Structural Framework .....	11
5.3 3D Property Modelling .....	11
5.3.1 Upscale Well-Log Data.....	11
5.3.2 Transform Upscaled Data.....	11
5.3.3 Variogram Modelling.....	11
5.3.4 Populate 3D Geocellular Grid.....	16
6 Model Quality.....	28
7 Observations .....	31
8 Model Outputs .....	44
9 Summary Remarks.....	44
10 References.....	45

## Tables

Table 1. Variogram parameters for the shale volume variable in the 3D property model.....	13
Table 2. Variogram parameters for the density porosity variable in the 3D property model. ....	14
Table 3. Variogram parameters for the water saturation variable in the 3D property model. ....	15

## Figures

Figure 1. Location of the study area and bedrock geology map. ....	2
Figure 2. Partial Table of Formations .....	3
Figure 3. Previously described Cardium Formation stratigraphy. ....	4
Figure 4. Well-log cross-section showing the gamma-ray, bulk density and deep resistivity logs. ....	6
Figure 5. Well-log cross-section showing the calculated shale volume, density porosity and water saturation logs. ....	10
Figure 6. Variogram model for the shale volume variable .....	13
Figure 7. Variogram model for the density porosity variable.....	14
Figure 8. Variogram model for the water saturation variable.....	15
Figure 9. Isometric view of two realizations for the shale volume model .....	17
Figure 10. Isometric view of the arithmetic mean of 100 realizations (top) and the kriging model (bottom) for the shale volume model .....	18
Figure 11. Isometric view of the 10 <sup>th</sup> (top) and 90 <sup>th</sup> (bottom) percentiles for the shale volume model.....	20
Figure 12. Isometric views of the fence diagram of the kriged shale volume model .....	21
Figure 13. Isometric view of two realizations for the density porosity model.....	22

Figure 14. Isometric view of the arithmetic mean of 100 realizations (top) and the kriging model (bottom) for the density porosity model.....	23
Figure 15. Isometric view of the 10 <sup>th</sup> (top) and 90 <sup>th</sup> (bottom) percentiles for the density porosity model .	24
Figure 16. Isometric view of the fence diagram for the density porosity model .....	25
Figure 17. Isometric view of two realizations for the water saturation model.....	26
Figure 18. Isometric view of the arithmetic mean of 100 realizations (top) and the kriging model (bottom) for the water saturation model.....	27
Figure 19. Isometric views of the fence diagram of the kriged water saturation model .....	28
Figure 20. Isometric view of the kriging standard deviation for the shale volume model (left), the density porosity model (middle) and the water saturation model (right).....	30
Figure 21. The 7 <sup>th</sup> slice of the kriged shale volume model .....	32
Figure 22. The 11 <sup>th</sup> slice of the kriged shale volume model and the lower Cardium Formation paleogeographic map .....	33
Figure 23. The 15 <sup>th</sup> slice of the kriged shale volume model and the middle Cardium Formation paleogeographic map .....	34
Figure 24. The 19 <sup>th</sup> slice of the kriged shale volume model and the upper Cardium Formation paleogeographic map .....	35
Figure 25. Comparison of the 23 <sup>th</sup> slice of the kriged shale volume model.....	36
Figure 26. Cross-sections of the kriged shale volume model. Location of the cross-section is indicated by line 6 (upper) and line 2 (lower) in Figure 1 .....	38
Figure 27. Cross-sections of the kriged shale volume model. Location of the cross-section is indicated by line 7 (upper) and line 3 (lower) in Figure 1 .....	39
Figure 28. Cross-sections of the kriged density porosity model. Location of the cross-section is indicated by line 6 (upper) and line 2 (lower) in Figure 1 .....	40
Figure 29. Cross-sections of the kriged density porosity model. Location of the cross-section is indicated by line 7 (upper) and line 3 (lower) in Figure 1 .....	41
Figure 30. Cross-sections of the kriged water saturation model. Location of the cross-section is indicated by line 6 (upper) and line 2 (lower) in Figure 1 .....	42
Figure 31. Cross-sections of the kriged water saturation model. Location of the cross-section is indicated by line 7 (upper) and line 3 (lower) in Figure 1 .....	43

## **Acknowledgements**

The authors wish to thank Steven Lyster, Kristine Haug, Sarah Schultz, and Matt Grobe for technical and editorial reviews.

## Abstract

A three-dimensional (3D) property model of sandiness/shaliness, porosity, and water saturation was developed for the Upper Cretaceous Cardium Formation in west-central and southern Alberta. The Cardium Formation is represented by a terrigenous, muddy, sandy, and conglomeratic siliciclastic wedge that is encased in black mudstones deposited during the period of maximum inundation of the Mesozoic North American foreland basin, forming one of the largest conventional light/medium oil deposits in Canada. The shale volume in the Cardium Formation is inversely related to the sandstone abundance and was calculated from gamma-ray logs from oil/gas wells. The porosity was calculated from bulk density logs and the water saturation from a combination of the gamma-ray, bulk density, and deep resistivity logs. The 3D property model covers an area of about 90 000 km<sup>2</sup> and represents an eastward-thinning wedge with a present-day maximum thickness of ~150 m in the foothills of the Canadian Rocky Mountains and thinning out towards the Alberta Plains and grading into mudstone along its easternmost terminus. Several trends emerge from the 3D modelling for the Cardium Formation in the subsurface of west-central and southern Alberta, including:

- The sandstone abundance generally decreases from northwest to southeast.
- In contrast to the sandstone abundance, the total porosity generally increases from northwest to southeast.
- The water saturation also generally increases from northwest to southeast.
- Sandstone and conglomerate are most abundant in the middle Cardium Formation. This interval can be clearly recognized in the cross-sections of the 3D property model for shale volume, density porosity, and water saturation.

The 3D property model was created in Schlumberger's Petrel 2017 and is available on the website of the Alberta Geological Survey ([https://ags.aer.ca/data-maps-models/MOD\\_2020\\_01.html](https://ags.aer.ca/data-maps-models/MOD_2020_01.html)). It illustrates the heterogeneity of shale volume, porosity, and water saturation in the Cardium Formation. It helps reveal depositional environments, history, and stacking patterns and provides insight to vertical and lateral connectivity of sandstone units. The resolution and accuracy of the 3D property model is constrained by the uncertainty and quality of the input logs and the methods used in modelling; as a result, the model is appropriate for regional-scale (1:100 000) assessments rather than site-specific investigations.

# 1 Introduction

Oil pools found in the Upper Cretaceous Cardium Formation of the Western Canada Sedimentary Basin have been producing oil since 1953 and represent one of the largest conventional light/medium oil deposits in Canada (Nielsen and Porter, 1984; Krause et al., 1994; Hart and Plint, 2003). The Cardium Formation's dominant rock types are mudstone and sandstone, with small but important conglomerate fractions. The original oil production was predominantly through vertical wells drilled into a 1–3 m thick interval, mainly in areas where there were extensive conglomerates, within the sandstone of the Cardium Formation which allowed oil to drain to the producing wells (Peachey, 2014). These pools were producing oil through primary production and extensive water flooding (Nielsen and Porter, 1984; Krasey, 1985) and have been in a general production decline for decades. The introduction of horizontal, multistage hydraulic fracturing technologies in 2009 has led to a major revival of activity by facilitating the production of unconventional or tight oil resources found in lower quality portions of the Cardium Formation or halos surrounding the main conventional pools (Viau and Nielsen, 2010; Clarkson and Pedersen, 2011; Klein et al., 2012; Pedersen et al., 2013). These tight zones contain considerable amounts of light oil but are not connected to the flow system leading to a producing vertical well and did not allow for commercial rates of production. Since 2009, almost all wells drilled into the Cardium have been horizontal wells combined with multi-stage hydraulic fracturing. The horizontal wells can increase the area of contact with the oil reservoir by 100 000s of times and result in economic oil production rates in relatively poor reservoir rock (Peachey, 2014).

The objective of this project is to evaluate the sandiness, porosity, and water saturation of the Cardium Formation. A 3D model was created and the Cardium Formation is represented by the shale volume, porosity, and water saturation determined from oil- and gas-well gamma-ray, bulk density, and deep resistivity logs. The 3D model enhances the characterization of conventional and unconventional zones at a scale appropriate for regional assessments rather than site-specific investigations. This report presents the results and methodology used to model the properties of the Cardium Formation in the subsurface of west-central and southwestern Alberta.

## 1.1 Study Area

The Cardium Formation is exposed in outcrop along the Rocky Mountain Foothills and present in the subsurface of the Alberta Plains. In plan view the formation is arranged in an arcuate strip, approximately 1000 km long, that swings through a 90 degree arc from Waterton Lakes National Park and Canada-U.S. border, past Grande Prairie, Alberta and beyond to Dawson Creek, British Columbia (Figure 1). We used the extent of the Cardium Formation from version two of the 3D Provincial Geological Framework (3D PGF v2) (Alberta Geological Survey, 2019) as the study area for the project (Figure 1). The study area covers 90 000 km<sup>2</sup> and is located in west-central and southwestern Alberta. The southwestern boundary of the study area is defined by the Cordilleran deformation belt.

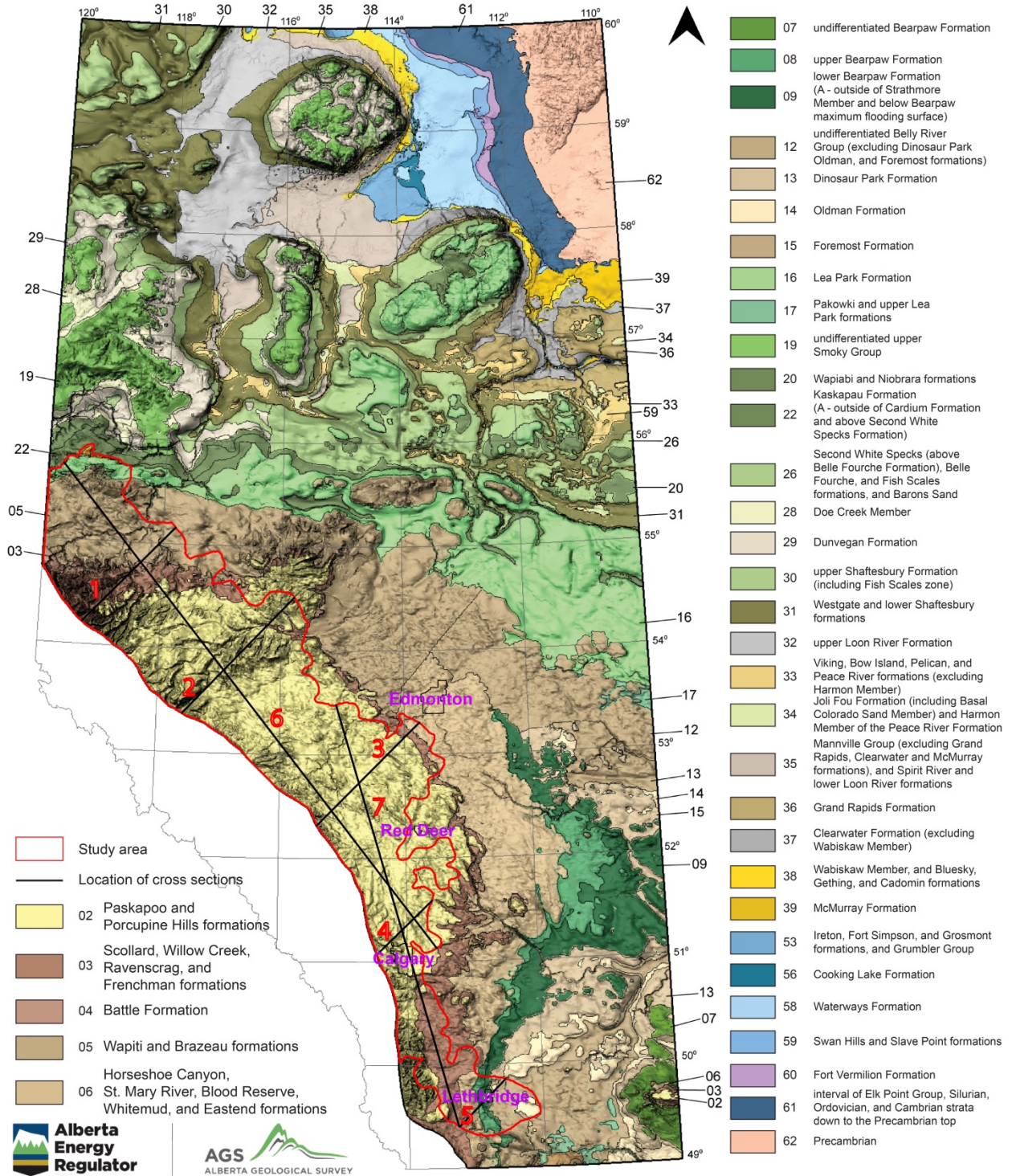


Figure 1. Location of the study area and bedrock geology map (modified from Alberta Geological Survey, 2019). Cross-section lines 1 to 7 (labelled in red) are referenced in subsequent figures.

## 2 Stratigraphic Framework

The term Cardium Formation was originally used to describe three thin sandstones between two thick shale packages outcropping along the Bow River (Rutherford, 1927). It was deposited during the latest Turonian to earliest Coniacian stages of the Late Cretaceous along the western margin of the Alberta Foreland Basin (Figure 2; Hall et al., 1994; Ogg and Hinnov, 2012). The Cardium Formation forms a terrigenous, muddy, sandy, and conglomeratic siliciclastic wedge which projects approximately 200 km into the basin's interior from the British Columbia-Alberta boundary. The Cardium Formation is 150 m thick in foothills exposures, thins in the subsurface of the plains to less than 50 m, and becomes indistinct along its easternmost terminus, melding into the mudstones of Carlile Formation (Figure 2; Krause et al., 1994).

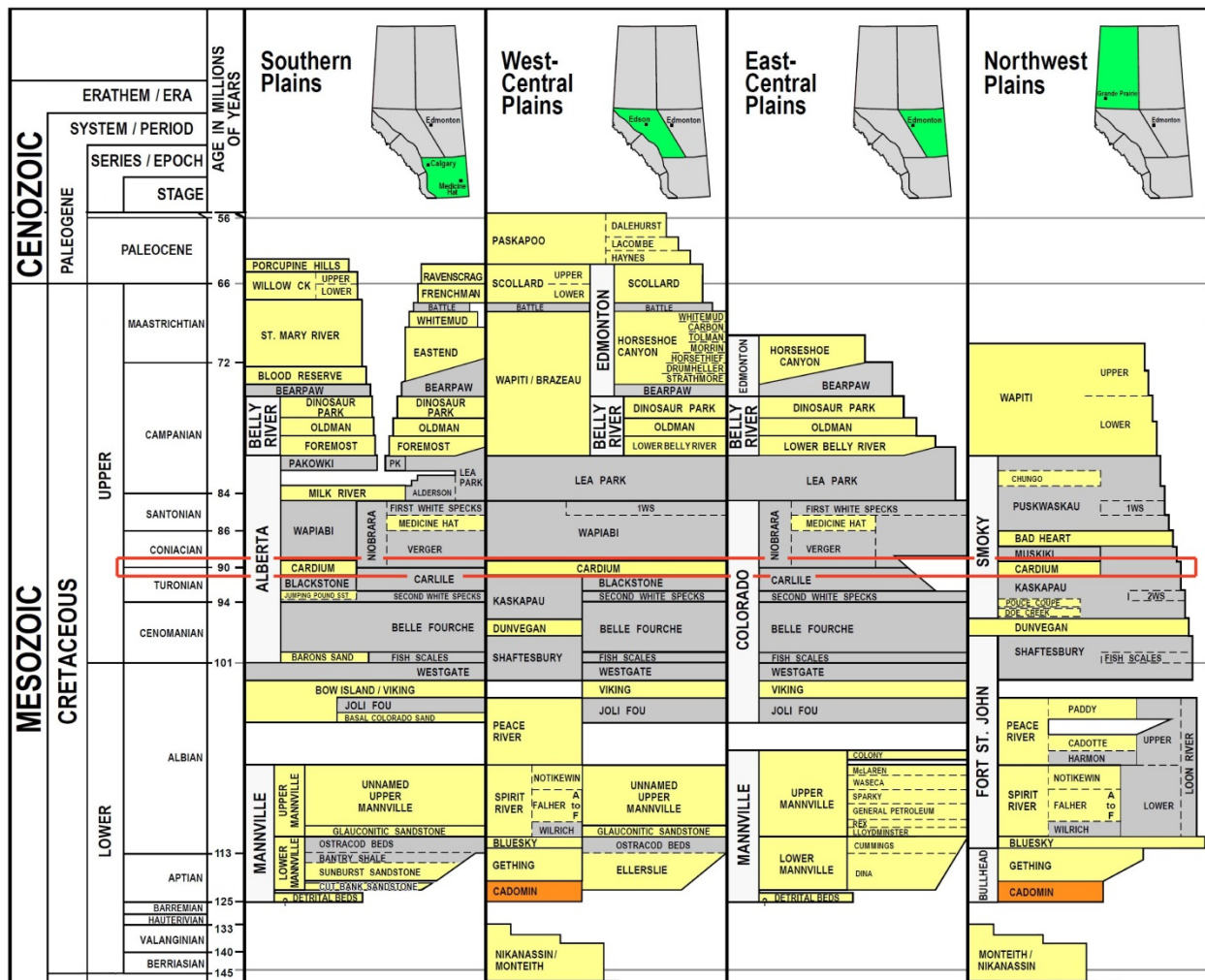


Figure 2. Partial Table of Formations (modified from Alberta Geological Survey, 2015). Cardium Formation and equivalent units are highlighted with the red rectangle.

The Cardium Formation is of significant geological interest because it represents a complex stratotectonic pulse during the period of maximum inundation of the Mesozoic North American foreland basin. It is encased by black mudstones representing successions of the Wapiabi or Muskiki formations above and the Blackstone or Kaskapau formations below (Figure 2; Krause et al., 1994). These formations form the middle part of the Alberta Group in the southwest, the Smoky Group in the northwest and the Colorado

Group towards the east (Figure 2). The Alberta, Smoky, and Colorado groups were deposited within the Western Canada foreland basin during an approximately 25 to 30 million year period when global sea level was high (Caldwell, 1984; Haq et al., 1987). Sedimentation took place within an active foreland basin, adjacent to a tectonically active hinterland. During the highstands, warm Tethyan water from the Gulf of Mexico mixed with the cooler boreal water extending south from the Arctic to form a shallow epeiric seaway. This major marine inundation was coincident with a regional tectonic downflexing of the North American craton (Lambeck et al., 1987), and was separated by four major regressive pulses represented by the Peace River-Viking-Bow Island, Dunvegan, Cardium-Bad Heart, and Milk River formations in ascending order. The erosional and depositional events preserved within the Alberta/Colorado/Smoky groups reflect this intermix of tectonic and eustatic controls.

The Cardium Formation contains multiple disconformities, paraconformities and diastems of variable regional extent (Braunberger and Hall, 2001a, 2001b; Hall et al., 1994; Hart and Flint, 1993, 2003; Krause et al., 1994; Krause et al., 1995; Krause and Braunberger, 2016; Walker et al., 2012; Walker et al., 1995). Figure 3 shows four major stratigraphic classification schemes for the Cardium Formation that have been developed for rocks in the subsurface and correlation to outcrop. The stratigraphic subdivisions were mainly based on observations at outcrops and/or well-log cross-sections rather than regional correlation and mapping of rock properties from large datasets in 3D modelling.

This report is concerned with the Cardium Formation in the subsurface only and the Cardium Formation is not subdivided. The top of the Cardium Formation is defined as the Cardium Zone Marker, which is characterized by a simple, distinct shoulder on the resistivity log in what is an otherwise continuous mudstone interval of the overlying Wapiabi or Muskiki formations. The base of the Cardium Formation is defined by the Russian Marker, which is characterized by a widespread double shoulder on the resistivity log in what is an otherwise continuous mudstone interval of the underlying Blackstone or Kaskapau formations (Krause et al., 1994).

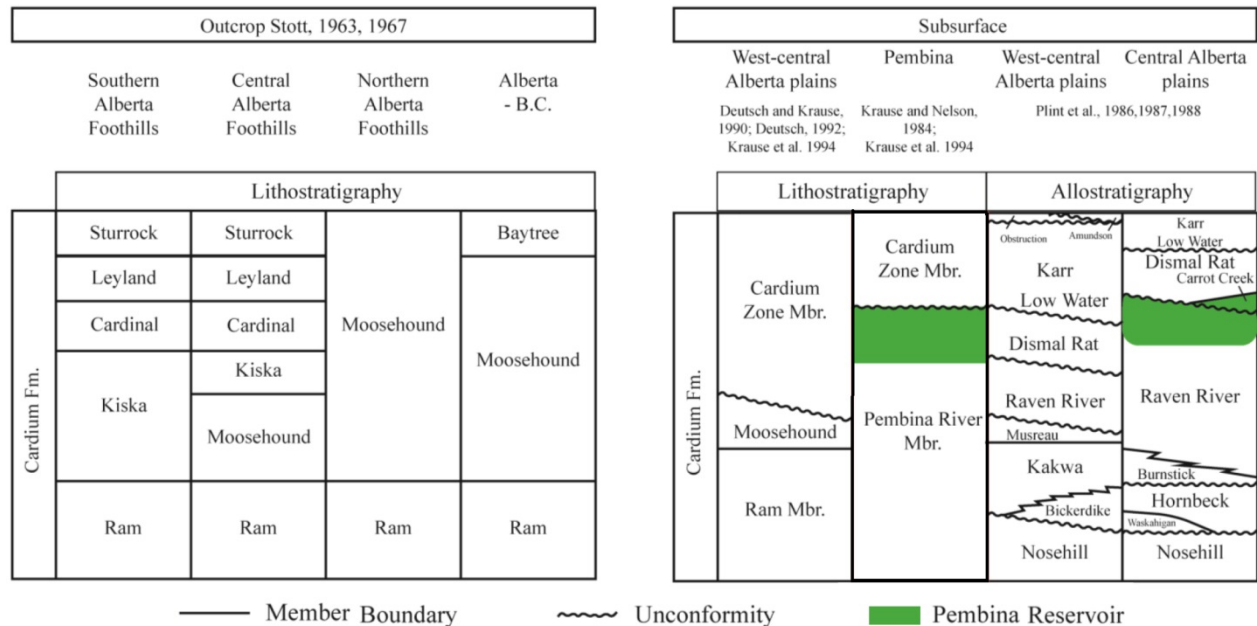


Figure 3. Previously described Cardium Formation stratigraphy (slightly modified from Wiseman, 2014).

### 3 Data and Compilation

In total, data from 9075 petroleum wells (current to October 23, 2014) were included in the project using LMKR GeoGraphix® PRIZM™ log analysis software. Well logs including gamma-ray, bulk density, and deep resistivity logs were imported from IHS™ AccuMap®.

4262 wells in total were found with a gamma-ray, a bulk density, and/or a deep resistivity log that cover the interval from Cardium Zone top to the Russian Marker; these wells were used for further analysis. They include 4110 wells with a gamma-ray log, 3590 wells with a bulk density log and 3388 wells with a deep resistivity log. Figure 4 is a cross-section showing an example of the well logs and the top and base surfaces of the Cardium Formation used.

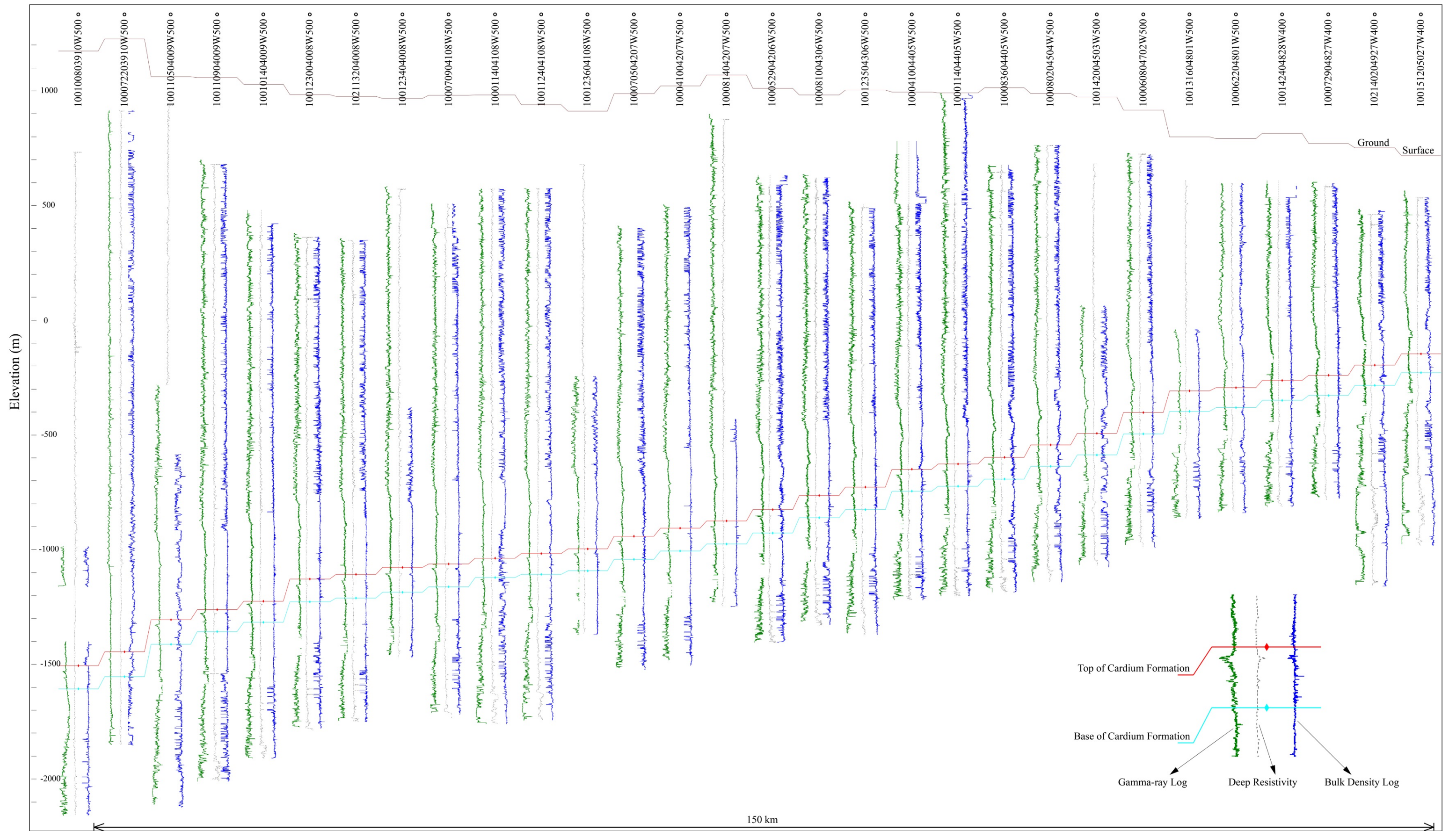


Figure 4. Well-log cross-section showing the gamma-ray, bulk density and deep resistivity logs used. The location of the cross-section is along the black line 3 in Figure 1.

## 4 Methods and Workflow

This section outlines the workflow for 3D property modelling using petroleum geophysical logs. This workflow includes steps from log analysis in LMKR GeoGraphix® PRIZM™ and populating properties in Schlumberger's 2017 Petrel E&P software within a 3D geocellular grid after a geological model construction is complete.

### 4.1 Log Analysis

#### 4.1.1 Shale Volume Calculation

A linear estimation method for shale volume from the gamma-ray log was used and the equation is:

$$VSH = (GR - GR_{sand}) / (GR_{shale} - GR_{sand})$$

where:

GR = gamma-ray log reading in zone of interest

GR<sub>sand</sub> = gamma-ray log reading in 100% clean zone

GR<sub>shale</sub> = gamma-ray log reading in 100% shale

VSH = shale volume from gamma-ray log

This method requires first determining the gamma-ray values associated with a zone of clean sandstone having no shale (GR<sub>sand</sub>) and a zone of 100% shale (GR<sub>shale</sub>).

In this project, these two values were chosen based on the statistics of gamma-ray values of the logs for the Cardium Formation. We chose 15 API as the gamma-ray value for GR<sub>sand</sub> which is 45 API less than the mean of the minimum gamma-ray values of the logs for the Cardium Formation. We chose 140 API as the GR<sub>shale</sub> which is 8 API higher than the mean of the maximum gamma-ray values of the logs. This makes a 77.5 API gamma-ray log value correspond to 50% shale.

#### 4.1.2 Density Log Processing

The density correction log was used to exclude bulk density log values where the absolute density correction is greater than 0.2 g/cm<sup>3</sup>.

#### 4.1.3 Density Porosity Calculation

Total porosity was calculated from bulk density logs. The method is based on a linear bulk mixing law and the equation is:

$$TPOR = (RHOMA - RHOB) / (RHOMA - RHOF)$$

Where:

RHOB = density log reading in zone of interest

RHOMA = density log reading in 100% matrix rock

RHOF = density log reading in 100% formation fluid

TPOR = total porosity from density log without shale correction

The method requires density values for both the matrix (RHOMA) and formation fluid (RHOF). The sandstones of the Cardium Formation consist of framework grains including quartz, feldspar, siderite, calcite, dolomite, rhodochrosite, muscovite, and pyrite (XRD results from AER data holdings). The XRD core data confirms that the matrix is not pure quartz as a result the sandstone scale matrix density, 2.65 g/cm<sup>3</sup>, cannot be used and a new matrix density needs to be calculated. Based on statistical analysis of

XRD core data and calibration with core porosity a value of 2.68 g/cm<sup>3</sup> was assigned for RHOMA. The fluid density was set as 1 g/cm<sup>3</sup>.

#### **4.1.4 Water Saturation Calculation**

Calculation of total water saturation in the Cardium Formation requires effective porosity (PHIE), resistivity of shale (RSH) and formation water resistivity (Rw) in addition to shale volume (Vsh).

The bound water saturation (Swb) is needed to calculate the effective porosity (PHIE); it was estimated using the empirical formula adopted from Bob Everett of Everett Petrophysics Inc. (personal communication):

$$Swb = Vsh^2$$

Then, the PHIE is calculated as below:

$$PHIE = TPOR - Vwb$$

$$Vwb = TPOR * Swb$$

$$PHIE = TPOR * (1 - Swb) = TPOR * (1 - Vsh^2)$$

Where:

Vwb = bound water volume

Swb = bound water saturation

TPOR = total porosity

Vsh = shale volume

PHIE = effective porosity (shale corrected porosity)

The RSH in the Cardium Formation varies from well to well with higher values in the shales than in the sandstones. Based on the 77.5 API cutoff value of gamma ray, a RSH value of 2 ohmm was used in the sandstones and 10 ohmm in the shales.

A total of 156 wells with formation water resistivity (Rw) data (ranging from 0.167–4.29 ohmm at 25 degree Celsius) were collected from the Water Resistivity Catalogue (Canadian Well Logging Society, 2002) and AGS water chemistry data holdings.

The Rw data was converted to RwFm (Rw at formation temperature) in the following steps.

The formation temperature (FmTemp) was first generated from depth using the following gradient from Prizm:

$$FmTemp \text{ (Celsius)} = 17.5 + 0.02 * \text{Depth}$$

Then again from Prizm, the resistivity temperature correction was done using the following equation:

$$R2 = R1 * (T1 + 21.5) / (T2 + 21.5)$$

Where

R1 is the Rw at a given temperature (T1) in Celsius and R2 is RwFm and T2 is FmTemp in Celsius.

Finally, the RwFm was used in calculating the effective water saturation (SwE) using Crain's modified Simandoux Method (Crain, 1986):

$$\text{CurveC} = (1 - V_{\text{sh}})^a * R_{\text{wFm}} / ((\text{PHIE} + 0.0001)^m)$$

$$\text{CurveD} = \text{CurveC} * V_{\text{sh}} / (2 * \text{RSH})$$

$$\text{SwE} = ((\text{CurveD}^2 + \text{CurveC} / \text{ResD})^{0.5} - \text{CurveD})^{2/n}$$

$$\text{SwT} = 1 - ((\text{PHIE} * (1 - \text{SwE}) / \text{TPOR})$$

Where:

a = 1.0 (tortuosity factor)

m = 1.85 (cementation exponent)

n = 1.85 (saturation exponent)

Vsh = shale volume

RwFm = formation water resistivity corrected for formation temperature

PHIE = effective porosity (shale corrected porosity)

RSH = resistivity of shale

ResD = deep resistivity

RwFm = water resistivity at formation temperature

SwE = effective water saturation

SwT = total water saturation

## 5 3D Modelling in Petrel

### 5.1 Input Source Data

The input source data for the 3D modelling includes the shale volume logs derived from gamma-ray logs, porosity logs derived from bulk density logs, water saturation logs derived from shale volume, porosity, and deep resistivity logs. Figure 5 is a cross-section showing an example of the derived well logs and geological framework surfaces for the base and top of the Cardium Formation. The shale volume logs were derived from 4110 oil and gas wells, the density porosity logs from 3590 wells, and water saturation from 3388 wells. The geological framework surfaces are from the 3D PGF v2 (Alberta Geological Survey, 2019) and include the surface for the Russian Marker defining the base of Cardium Formation and the surface for the top of the Cardium Formation.

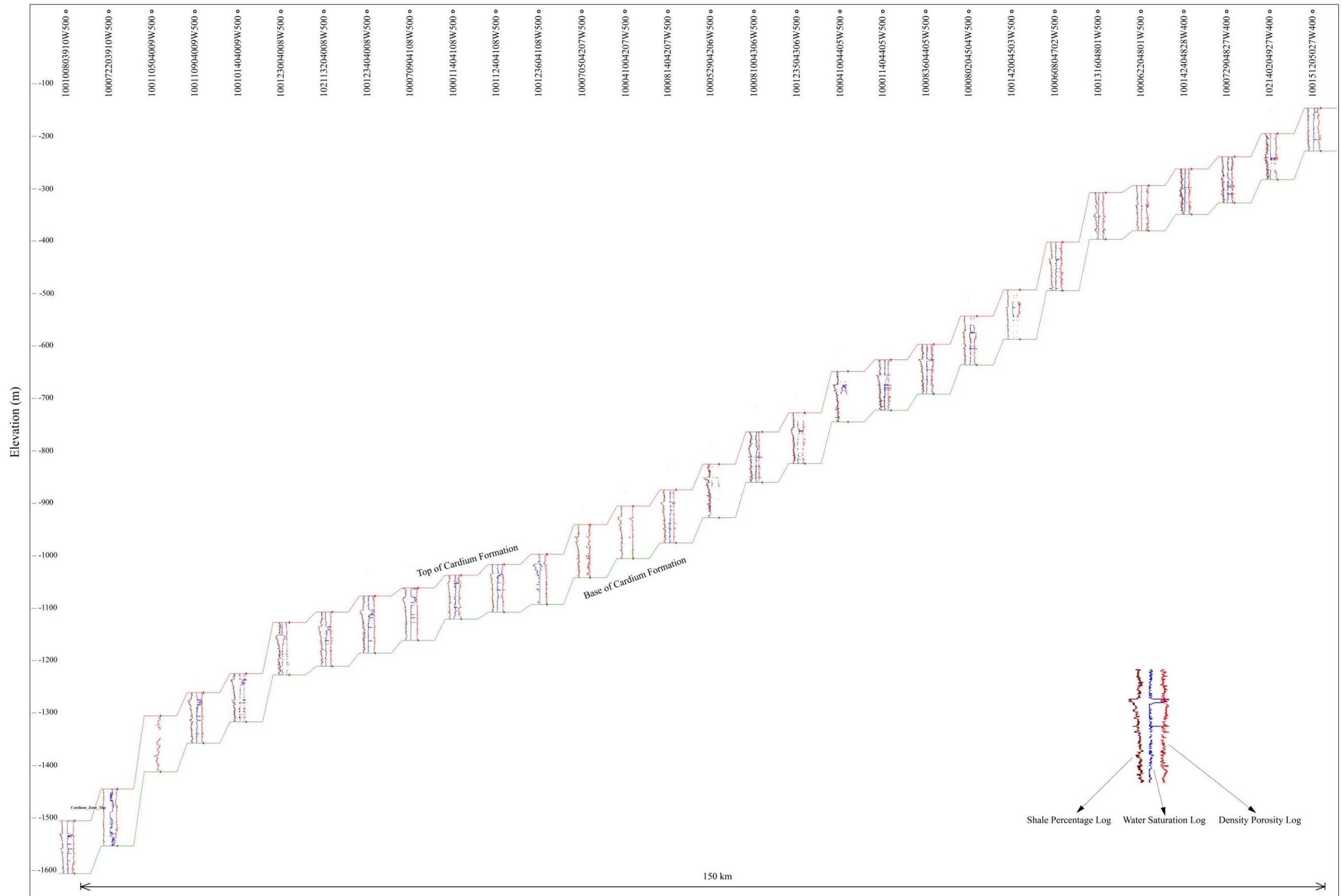


Figure 5. Well-log cross-section showing the calculated shale volume, density porosity and water saturation logs. The location of the cross-section is along the black line 3 in Figure 1.

## 5.2 Structural Framework

The base and top surfaces of the Cardium Formation from the 3D PGF v2 were used to define the top and basal boundaries of the 3D property model. The extent of the 3D property model is defined by the extent of the Cardium Formation as shown in Figure 1. The 3D model contains one zone with an average thickness of 85 m. We set the horizontal grid increment to 500 m x 500 m and divided the structural model vertically into layers to create a 3D geocellular model. The layers were created using the proportional layering option, which divides the model vertically into 34 layers with average layer thickness of about 2.5 m. At a horizontal grid of 500 m x 500 m and a vertical grid of nominally 2.5 m, the 3D geocellular model has 1066 x 1482 x 34 cells for a total of 53 713 608 grid cells, 12 072 083 of which have defined property values.

## 5.3 3D Property Modelling

The shale volume, density porosity and water saturation were modelled using geostatistical methods to populate the 3D geocellular model. The 3D property modelling includes five steps:

- Upscale the well-log data to the scale of the 3D geocellular grid.
- Transform the upscaled data to a normal score distribution.
- Calculate the experimental variograms for each normal score transformed variable.
- Fit variogram models to the experimental variograms.
- Populate the 3D geocellular grid using a geostatistical algorithm.

### 5.3.1 Upscale Well-Log Data

The well-log data for the shale volume, density porosity, and water saturation were recorded at very fine regular intervals (typically 6" or 15.2 cm). To model these properties in a 3D model where the cells are 500 x 500 x 2.5 m, the data were upscaled from the well logs to the geocellular model to facilitate the property modelling. In the upscaling process, the averaging of a data set from a scale of 15.2 cm to 2.5 m reduces the variance of the data distribution as the highest and lowest values are smoothed out.

### 5.3.2 Transform Upscaled Data

A normal score transformation was applied to the upscaled well-log data. This transformation makes the upscaled data follow a standard normal (Gaussian) distribution with a mean of zero, a variance of one, and a normal or bell-curve distribution. A back transformation restores the shape and units of the input distribution from the upscaled data values after the modelling is completed.

### 5.3.3 Variogram Modelling

The geostatistical methods used for property modelling require the spatial structure of the modelled variables to be quantified (Pyrzcz and Deutsch, 2014). A variogram quantifies the relationship between values at specified distances and this information is used to calculate the weights for data points used for estimation. An experimental variogram is calculated from data and then a variogram model function is fitted. For 3D property modelling, the variogram needs to be calculated and modelled in three directions: the major and minor horizontal directions, and the vertical direction. Each direction is modelled independently of the others, but with the same nested structures in the function.

A variogram model is needed for each variable in each zone or facies. Using shale volume variable as an example, variograms were calculated and modelled using a combination of functions with the major

direction of horizontal correlation at an azimuth of 158 degrees and the minor direction perpendicular to that. [Figure 6](#) shows the experimental and modelled variograms for the shale volume variable. The vertical direction displays zonal anisotropy, meaning the variogram does not appear to reach the sill of 1.0 for a very long distance. A spherical structure with a very short horizontal range was used to account for this. There is an apparent nugget effect in the horizontal directions that is higher than the apparent sill in the vertical direction. An exponential structure was used to account for this. The major horizontal direction shows zonal anisotropy; as a result, a Gaussian structure was used to capture the partial sill of the zonal anisotropy of the major horizontal direction and another Gaussian structure for the rest of the apparent sill. [Table 1](#) shows the parameters for the shale volume variogram modelling. [Figure 7](#) and [Table 2](#) show the experimental and modelled variograms and parameters for the porosity variable. [Figure 8](#) and [Table 3](#) show the experimental and modelled variograms and parameters for the water saturation variable.

**Figure 6. Variogram model for the shale volume variable. Top right: vertical direction; bottom left: major direction; bottom right: minor direction. Black squares: experimental variograms; blue lines: modelled variogram functions; red/green/purple/cyan squares: individual variogram function ranges and sills; grey line: least squares regression line; grey bars: number of variogram pairs at each lag.**

**Table 1. Variogram parameters for the shale volume variable in the 3D property model.**

Zone	Major horizontal direction	Structure	Model function	Sill	Vertical range	Major horizontal range	Minor horizontal range
Cardium Formation	158 degrees	0	Nugget	0.0001			
		1	Spherical	0.4168	25.251	500	500
		2	Exponential	0.1741	378.659	20909.049	20273.343
		3	Gaussian	0.048	378.659	87605.051	84483.887
		4	Gaussian	0.361	380.403	685494.936	141188.326

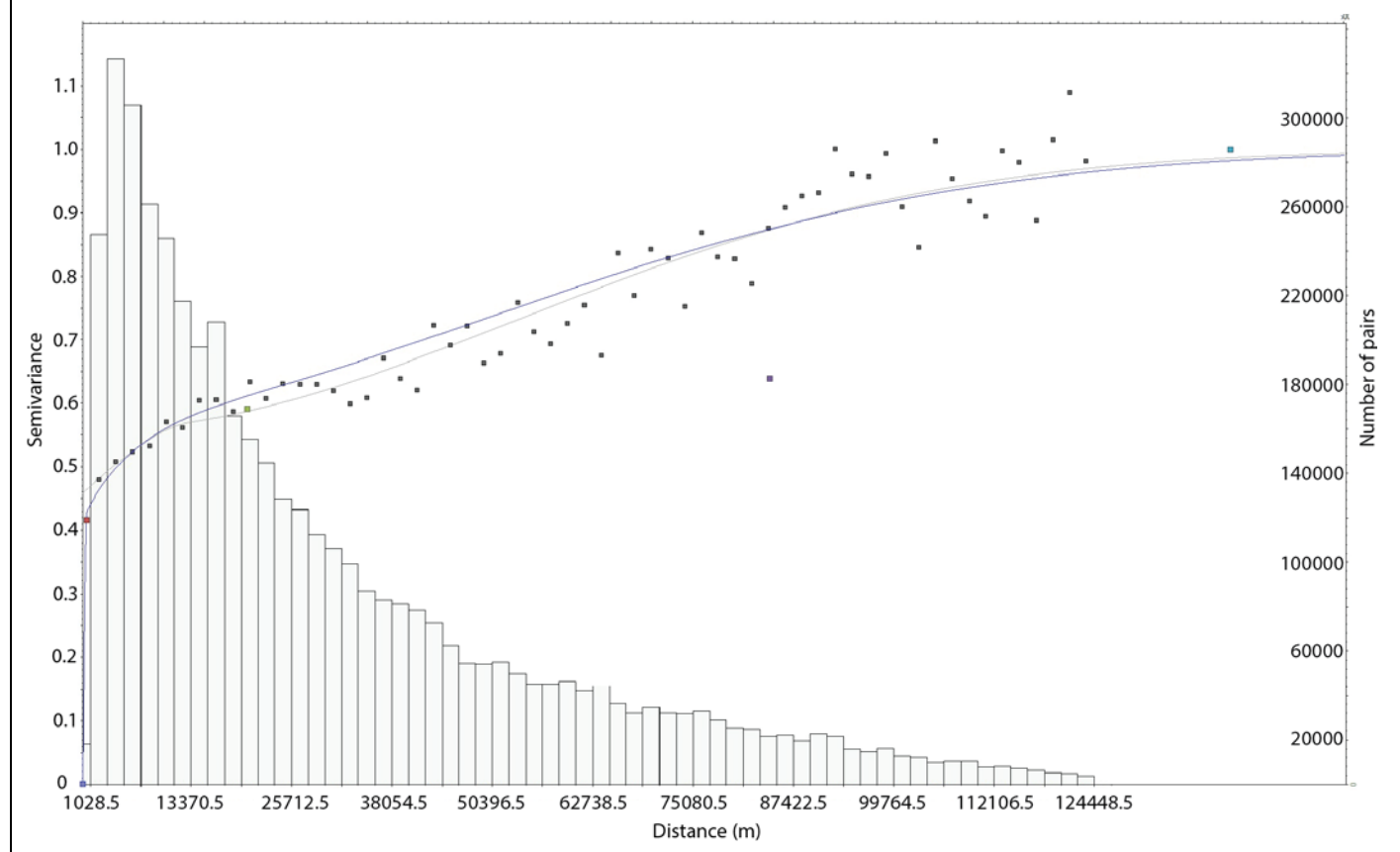
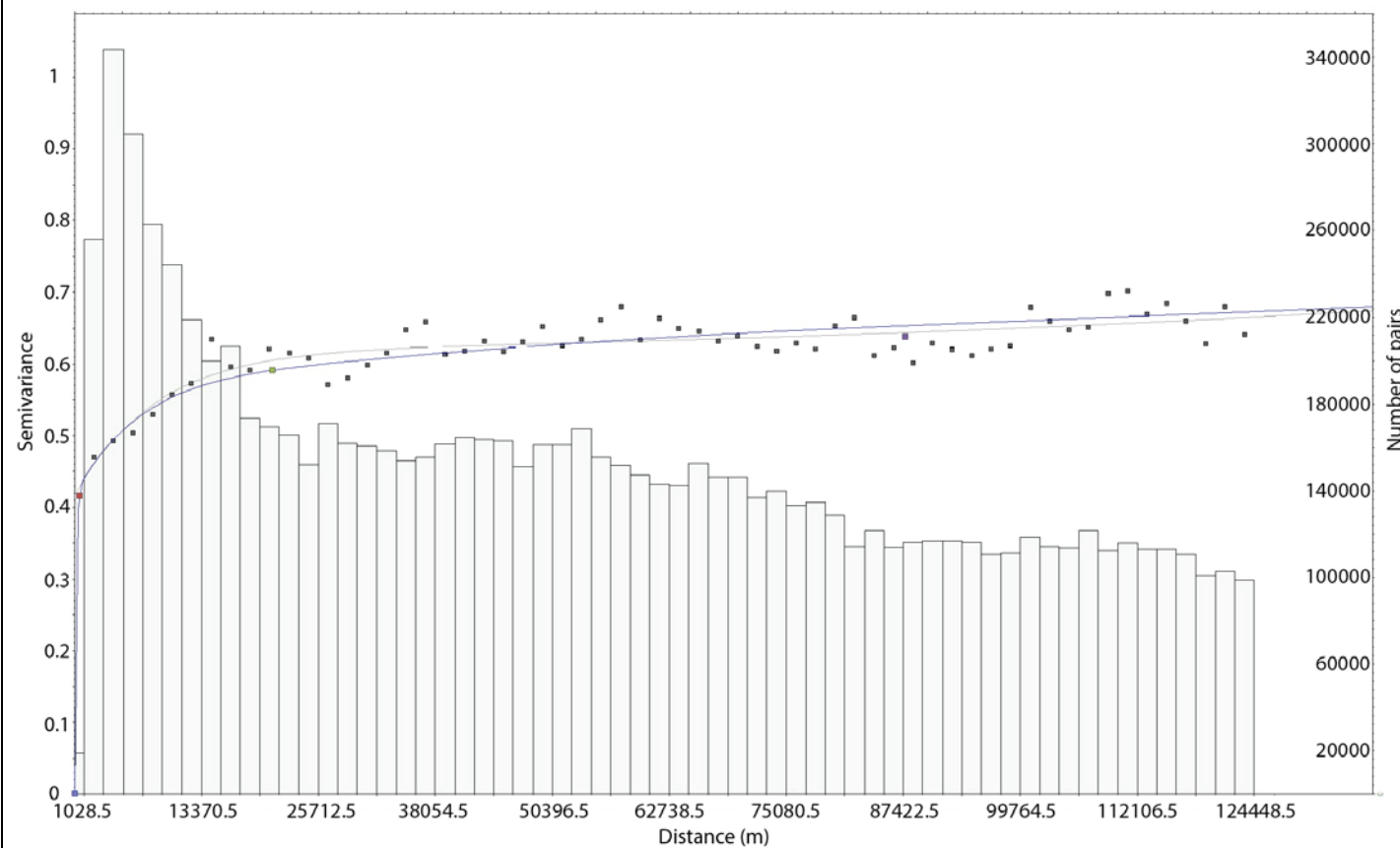
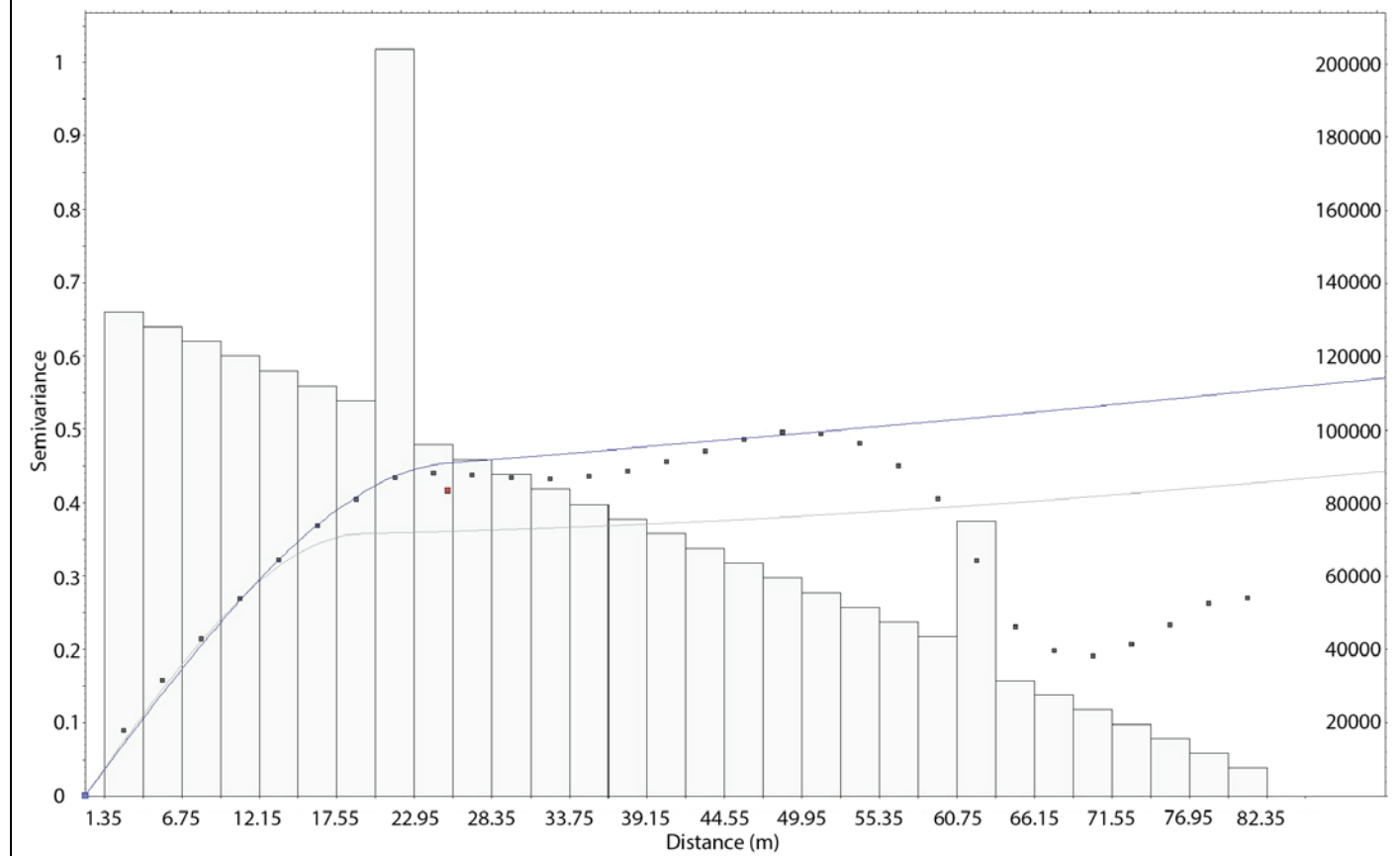


**Figure 7. Variogram model for the density porosity variable. Top right: vertical direction; bottom left: major direction; bottom right: minor direction. Black squares: experimental variograms; blue lines: modelled variogram functions; red/green/purple/cyan squares: individual variogram function ranges and sills; grey line: least squares regression line; grey bars: number of variogram pairs at each lag.**

**Table 2. Variogram parameters for the density porosity variable in the 3D property model.**

Zone	Major horizontal direction	Structure	Model function	Sill	Vertical range	Major horizontal range	Minor horizontal range
Cardium Formation	158 degrees	0	Nugget	0.1			
		1	Exponential	0.2706	25.117	355.733	344.206
		2	Exponential	0.4096	534.205	355.733	344.206
		3	Exponential	0.0802	558.808	14834.033	14750.644
		4	Gaussian	0.1396	596.046	229885.315	107411.665

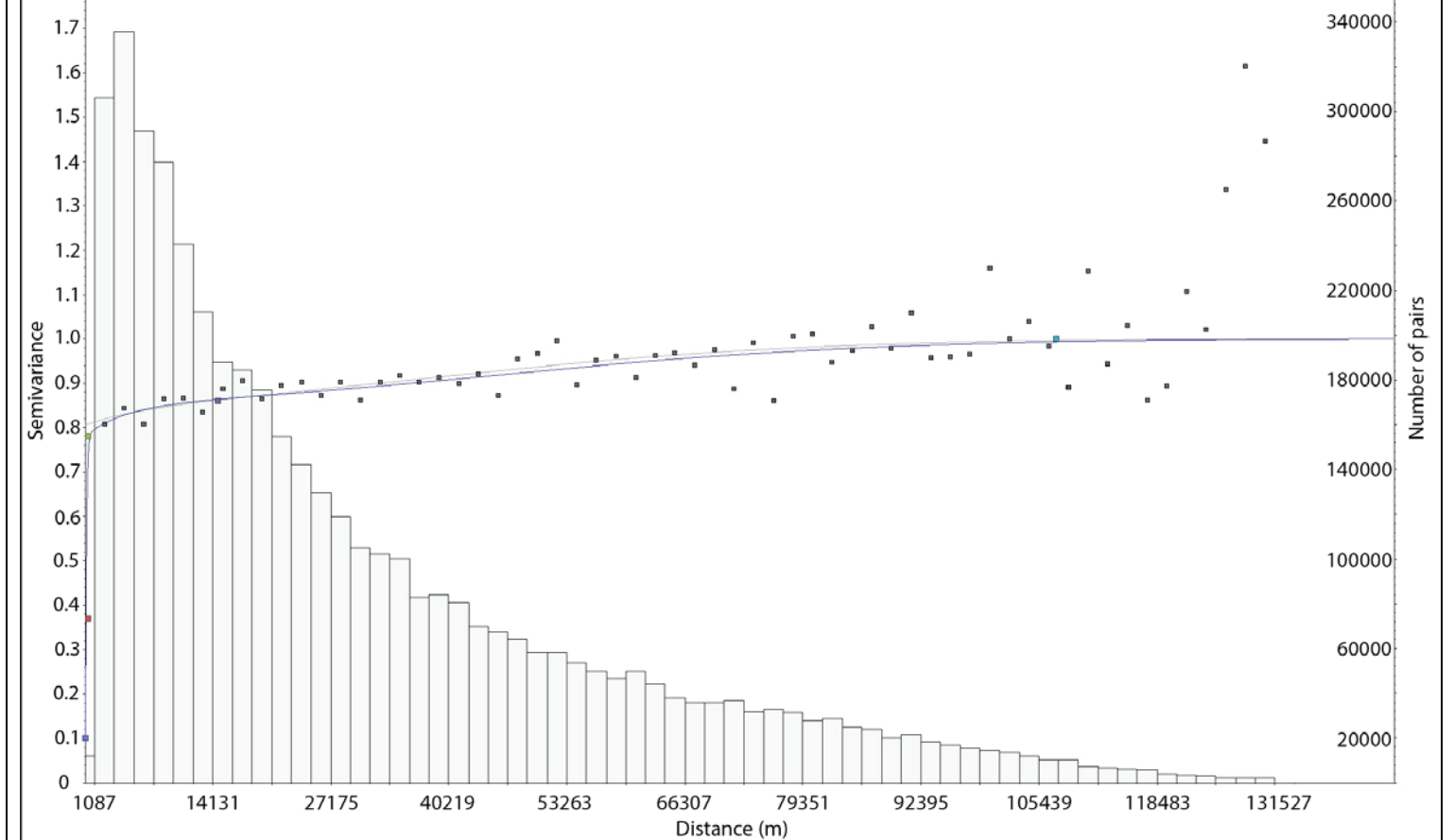
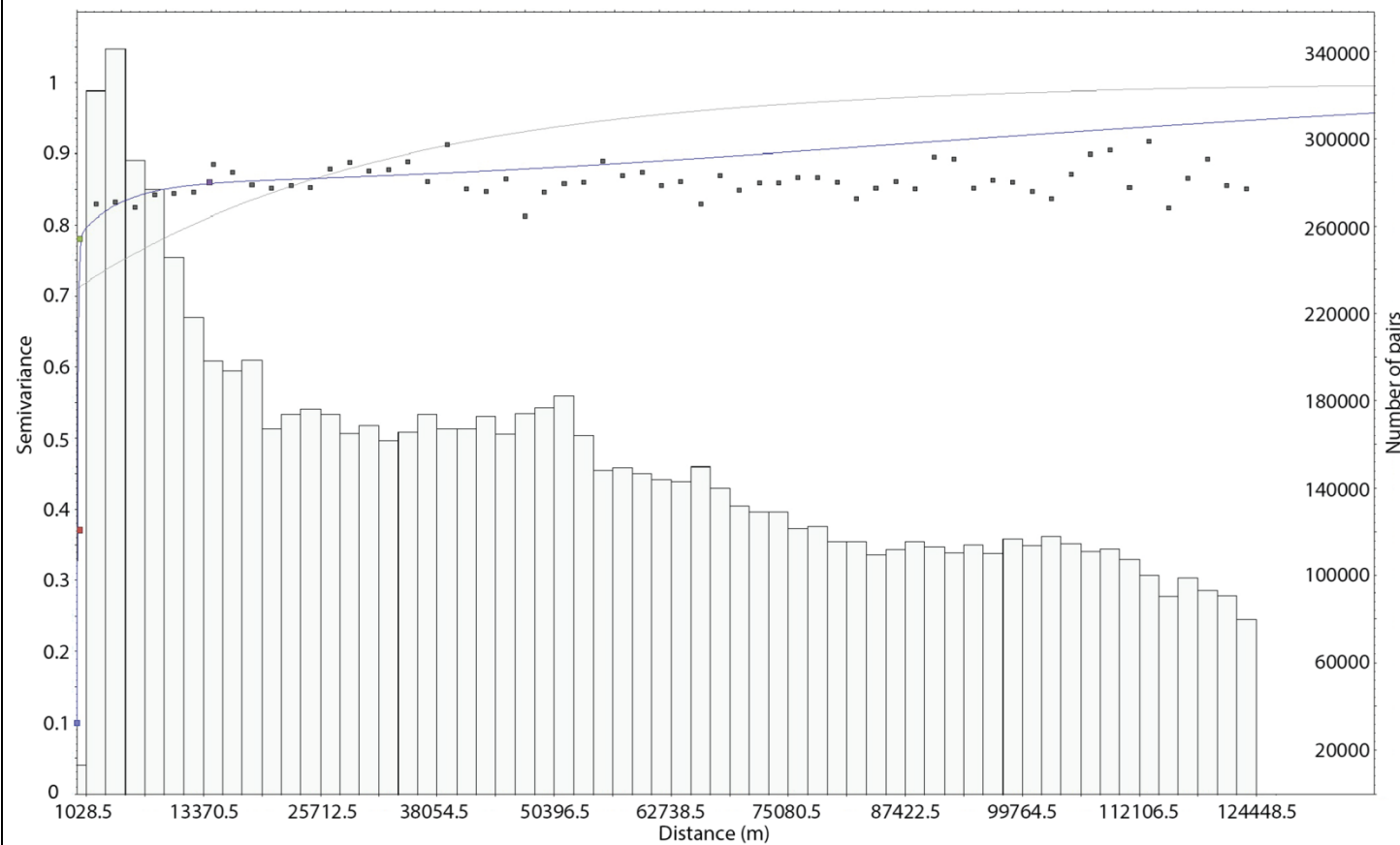
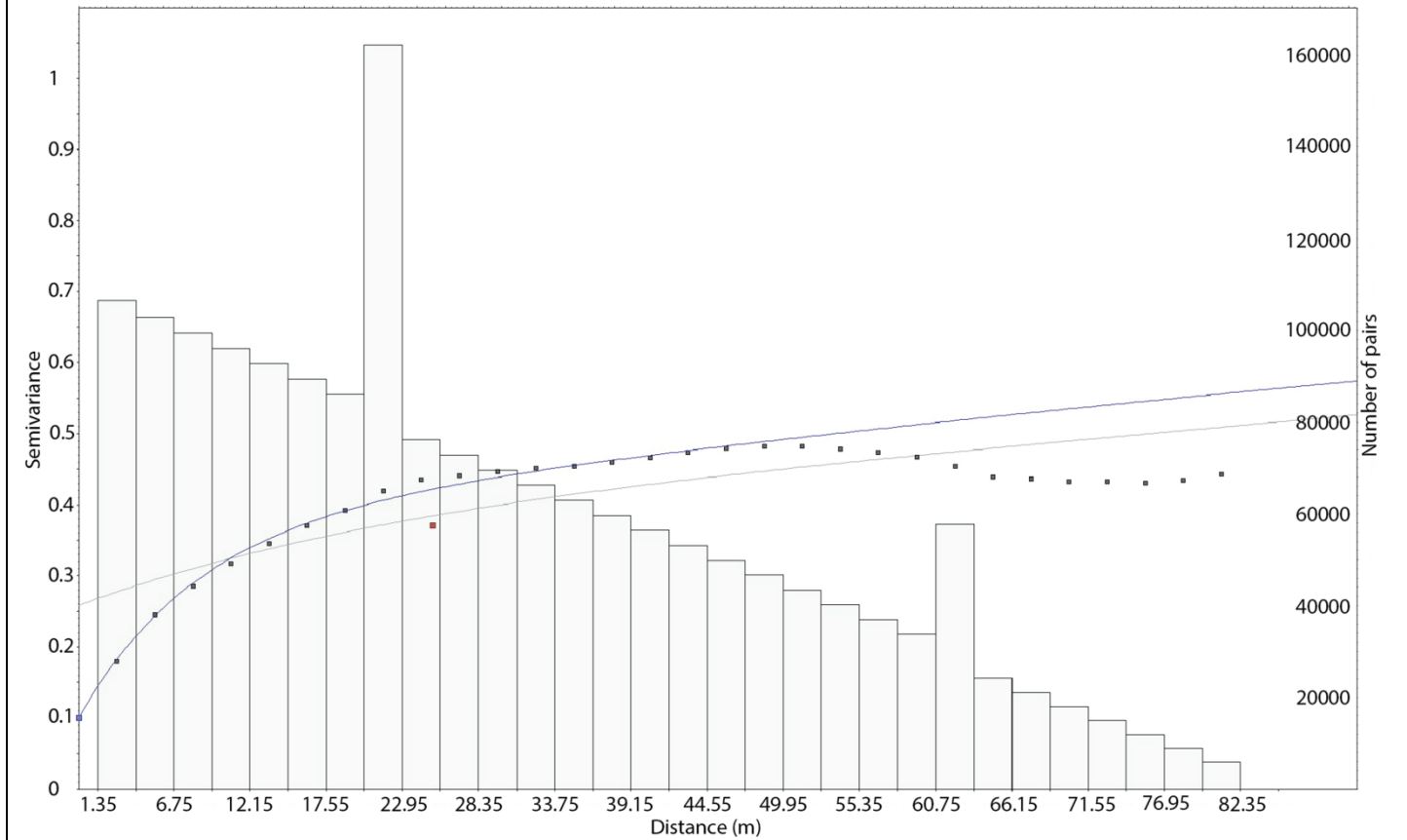
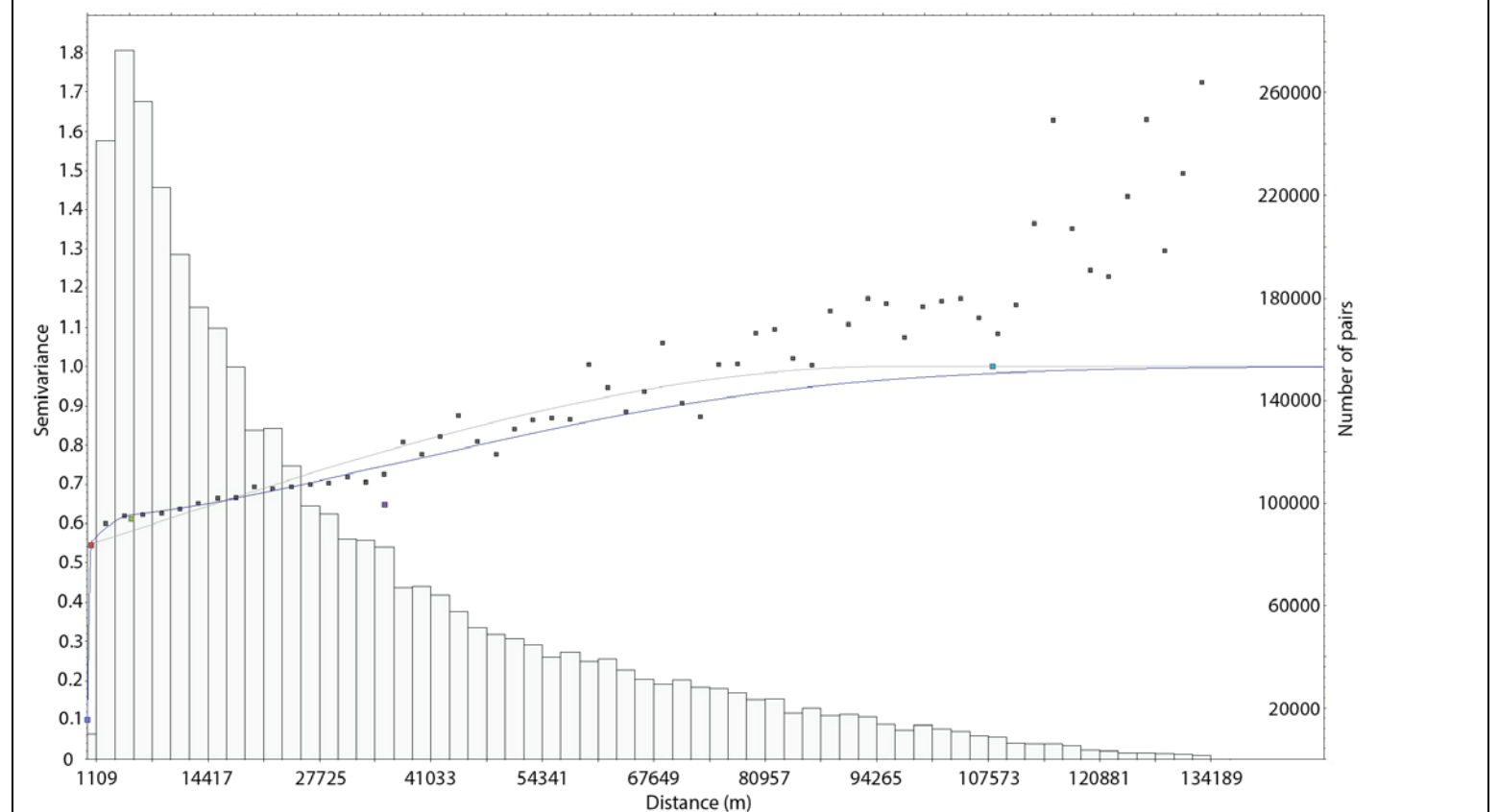
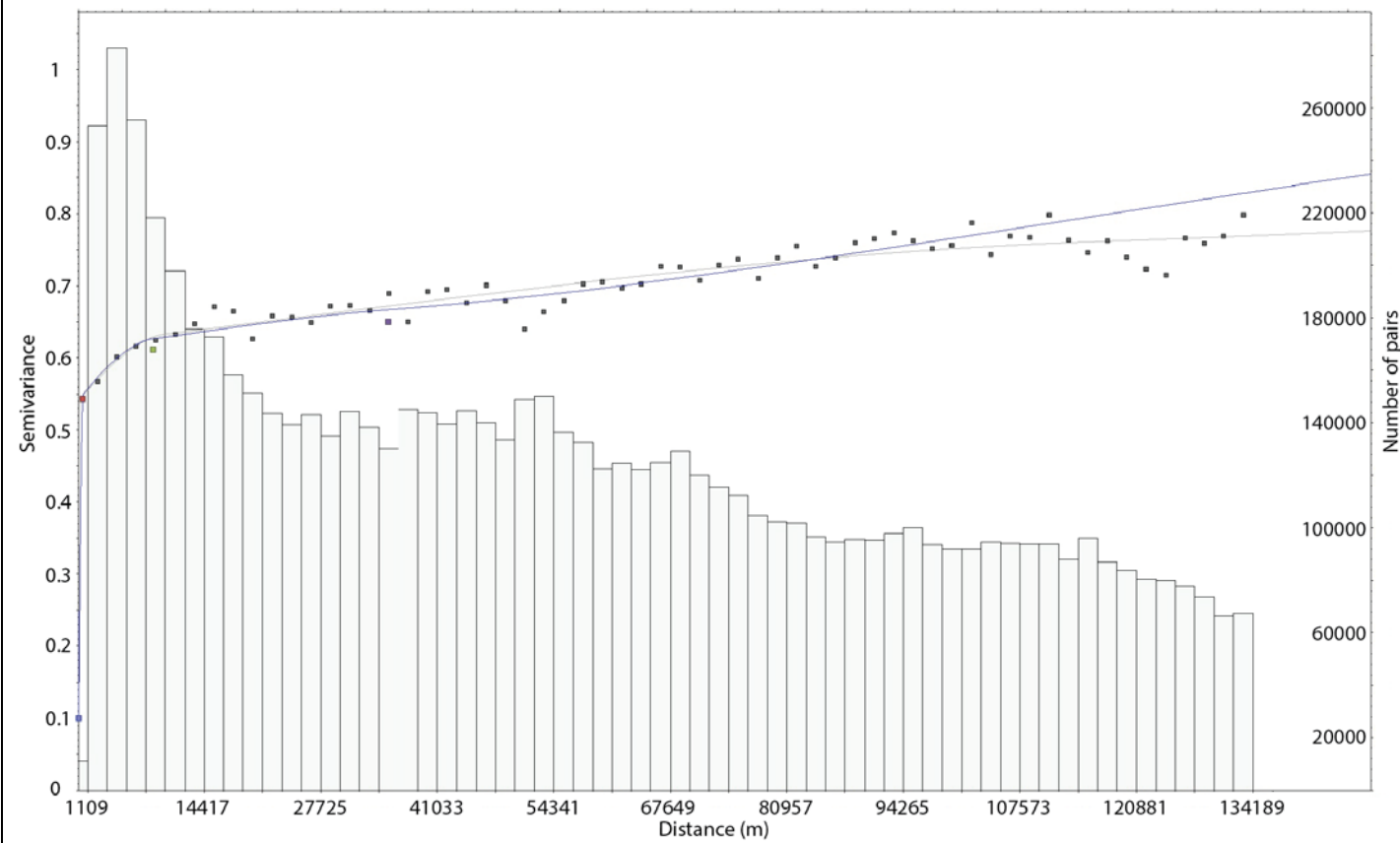
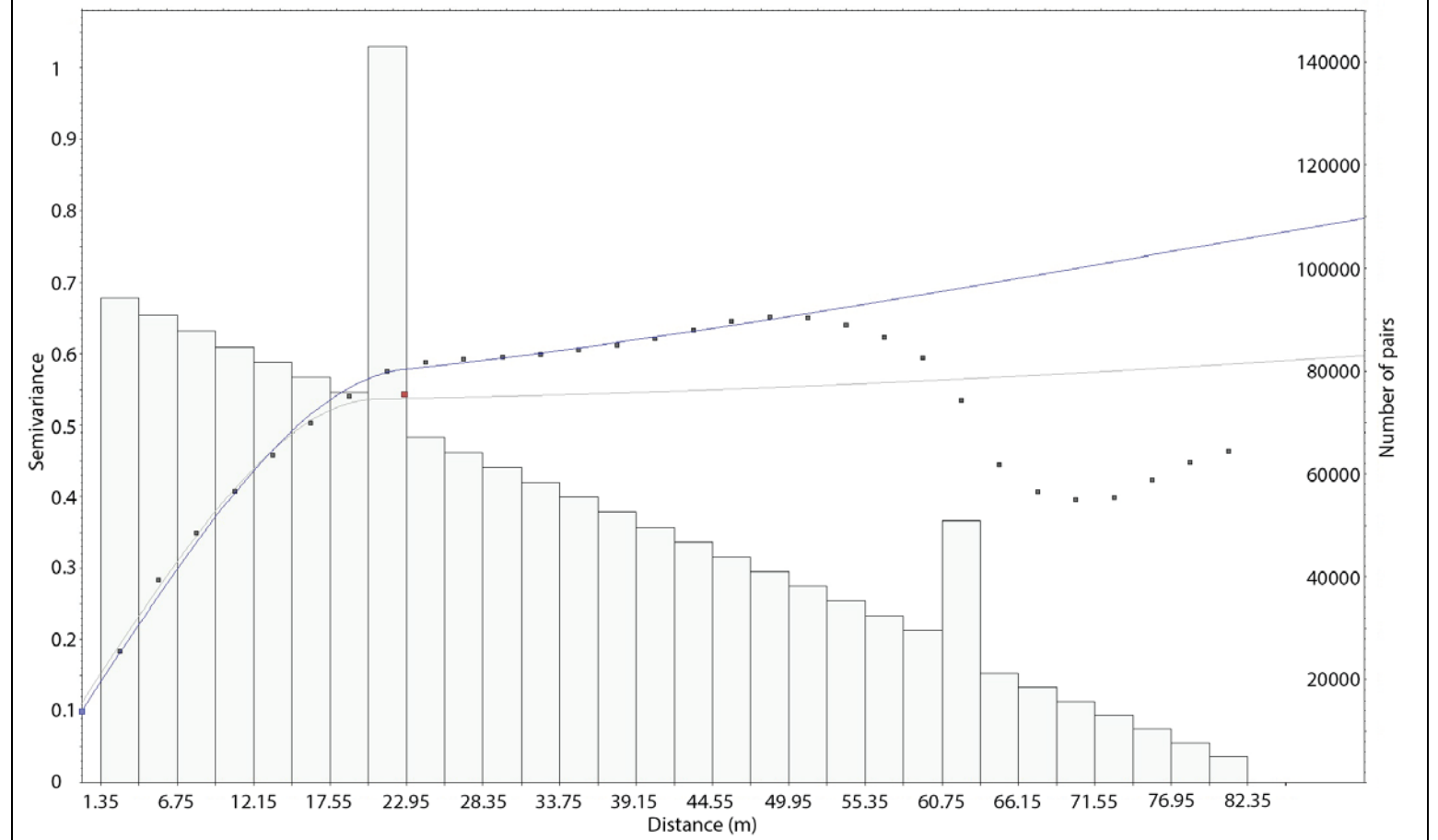


**Figure 8. Variogram model for the water saturation variable. Top right: vertical direction; bottom left: major direction; bottom right: minor direction. Black squares: experimental variograms; blue lines: modelled variogram functions; red/green/purple squares: individual variogram function ranges and sills; grey line: least squares regression line; grey bars: number of variogram pairs at each lag.**

**Table 3. Variogram parameters for the water saturation variable in the 3D property model.**

Zone	Major horizontal direction	Structure	Model function	Sill	Vertical range	Major horizontal range	Minor horizontal range
Cardium Formation	158 degrees	0	Nugget	0.1			
		1	Spherical	0.4434	22.794	500	500
		2	Spherical	0.0682	170.248	8584.001	5290.519
		3	Spherical 1	0.0381	191.412	35380.976	35530.677
		4	Gaussian	0.3503	191.412	272731.125	108136.998



### **5.3.4 Populate 3D Geocellular Grid**

The algorithm used in this study for property modelling is Gaussian Random Function Simulation (GRFS) (Daly et al., 2010) in Petrel. This geostatistical method is based on kriging (Pyrcz and Deutsch, 2014) to estimate the values and then add an unconditionally simulated random value to the kriging estimates to generate a realization that is conditional to the input data and correctly reproduces the variability in the original data.

[Figure 9](#) shows isometric views of two simulated realizations of the shale volume model, [Figure 10](#) shows isometric views of the arithmetic mean of 100 realizations and the kriged model. Each realization is different but equally probable and honours all of the data. The simulated realizations typically look “patchy” with a mixture of high and low values; however, the arithmetic mean of 100 realizations is smooth and nearly identical to the kriged model, with cell values tending towards the centre of the distribution.

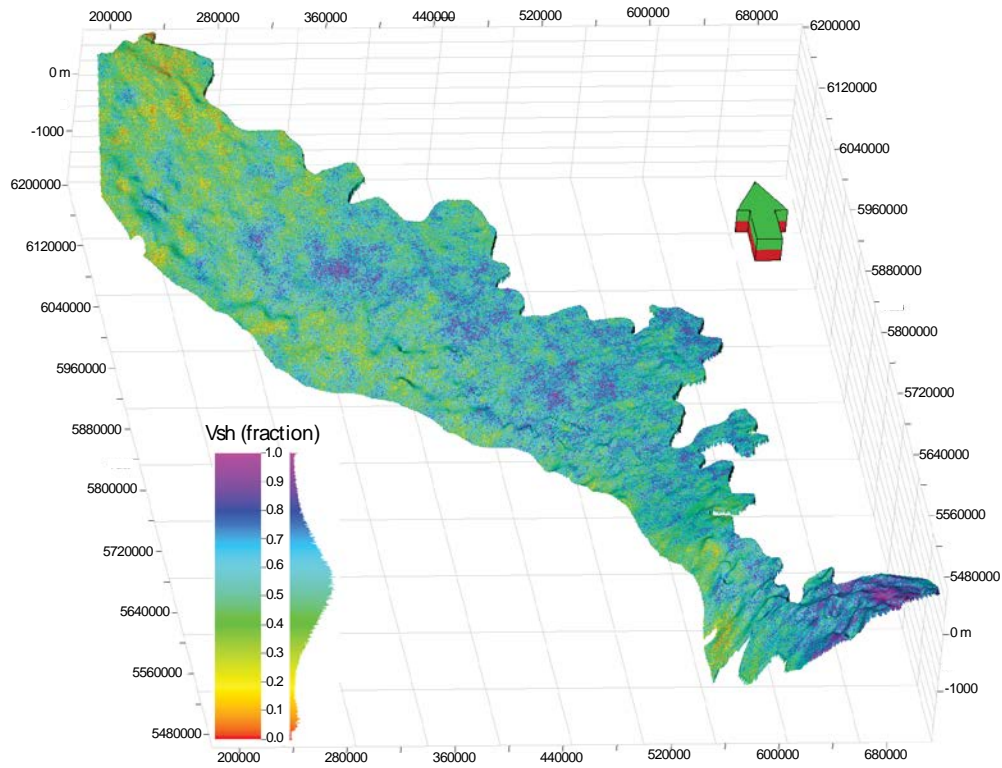
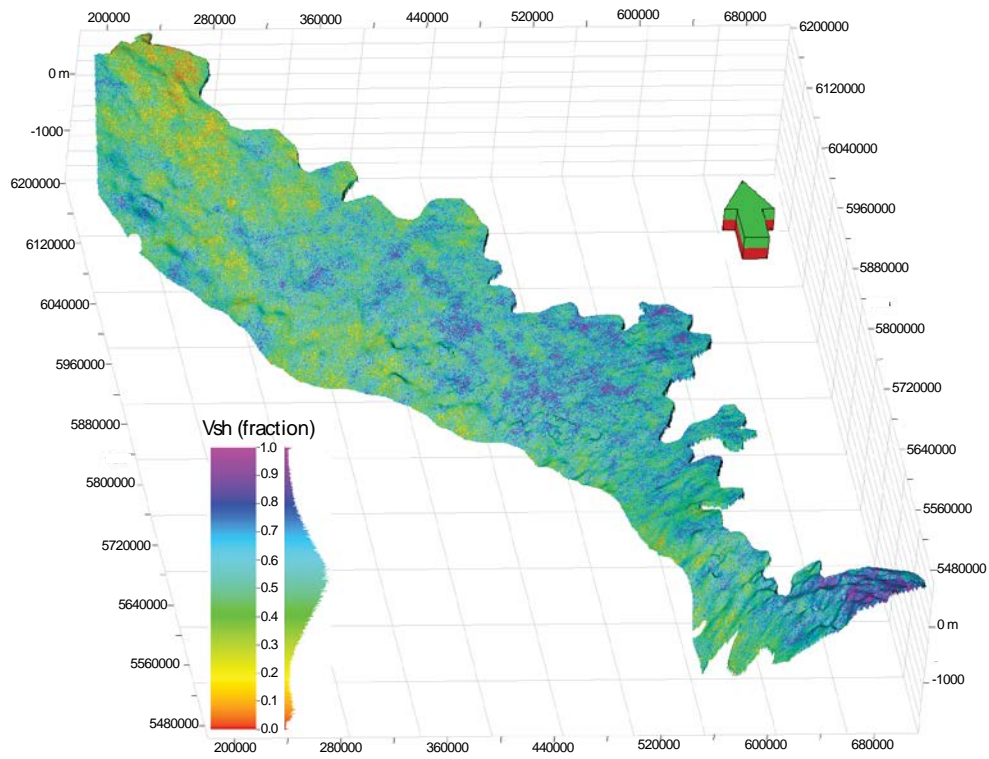


**Figure 9. Isometric view of two realizations for the shale volume model. Vertical exaggeration is 50 times.**

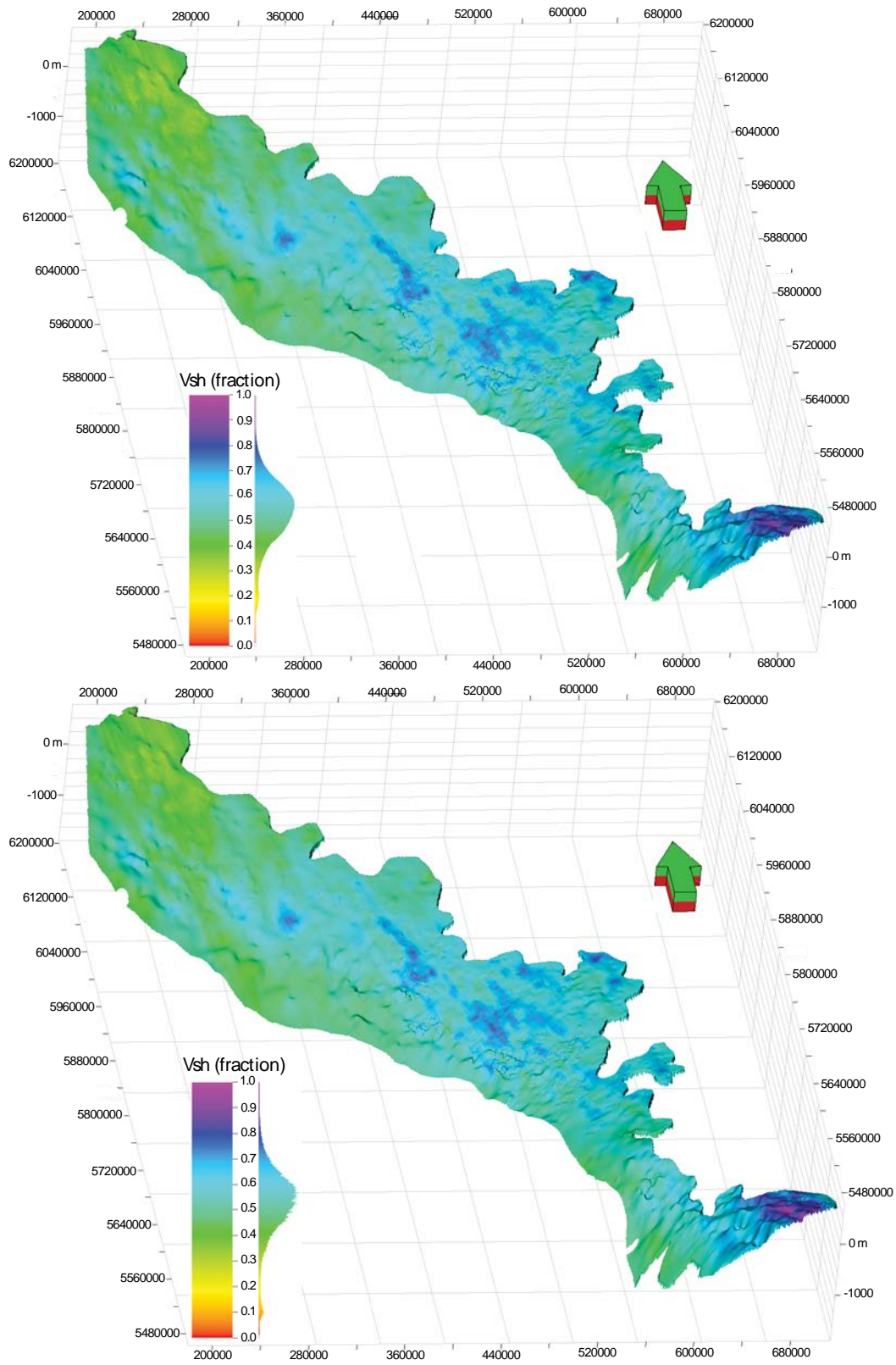


**Figure 10. Isometric view of the arithmetic mean of 100 realizations (top) and the kriging model (bottom) for the shale volume model. It shows that the sandstone abundance generally decreases from northwest to southeast. Vertical exaggeration is 50 times.**

The 100 simulated realizations allow the 10<sup>th</sup> percentile (P10) and 90<sup>th</sup> percentile (P90) to be calculated for each cell in the 3D model. [Figure 11](#) shows isometric views of the P10 and P90 models. The P10 model is commonly used to highlight areas with high possibility of high values because 90 out of 100 models predicted that the shale volume values could exceed the value at any locations in the P10 model. The P90 model is commonly used to highlight areas with high possibility of low values because 90 out of 100 models predicted that the shale volume values could be less than the value at any locations in the P90 model.

For example, the central-east and southeast areas of the model are represented as cyan to blue (relatively high shale volume) in the P10 model, indicating that these areas are more certain to be shale-dominated compared to other areas. The northwest area of the model is represented by cyan to green (relatively low shale volume) in the P90 model, indicating that this area is more certain to be sandstone-dominated compared to other areas.

[Figure 12](#) shows the isometric view of the fence diagrams of the kriged model of the shale volume to show how it varies regionally throughout the model area.

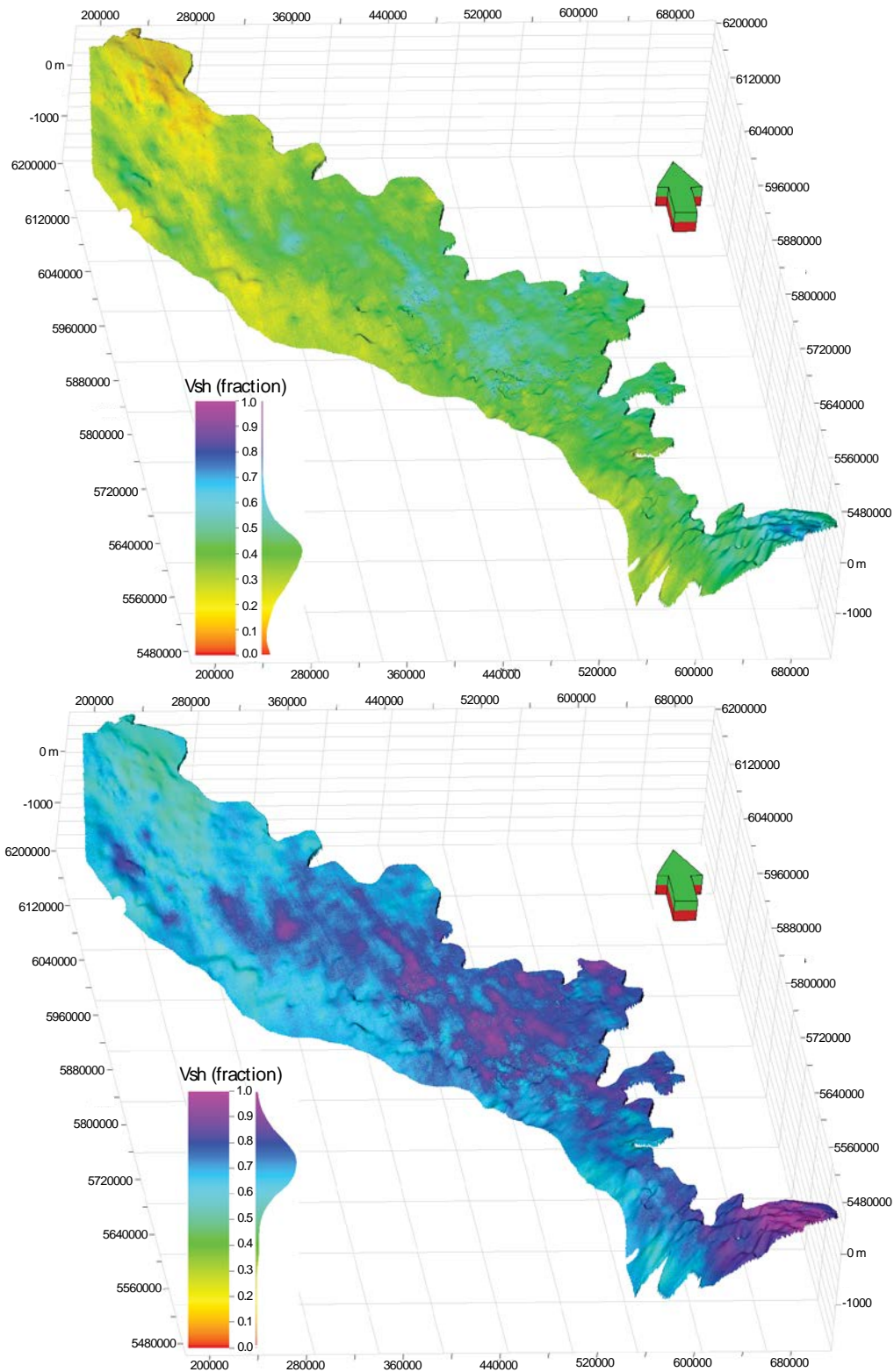


**Figure 11. Isometric view of the 10<sup>th</sup> (top) and 90<sup>th</sup> (bottom) percentiles for the shale volume model. It shows that the sandstone abundance generally decreases from northwest to southeast. Vertical exaggeration is 50 times.**

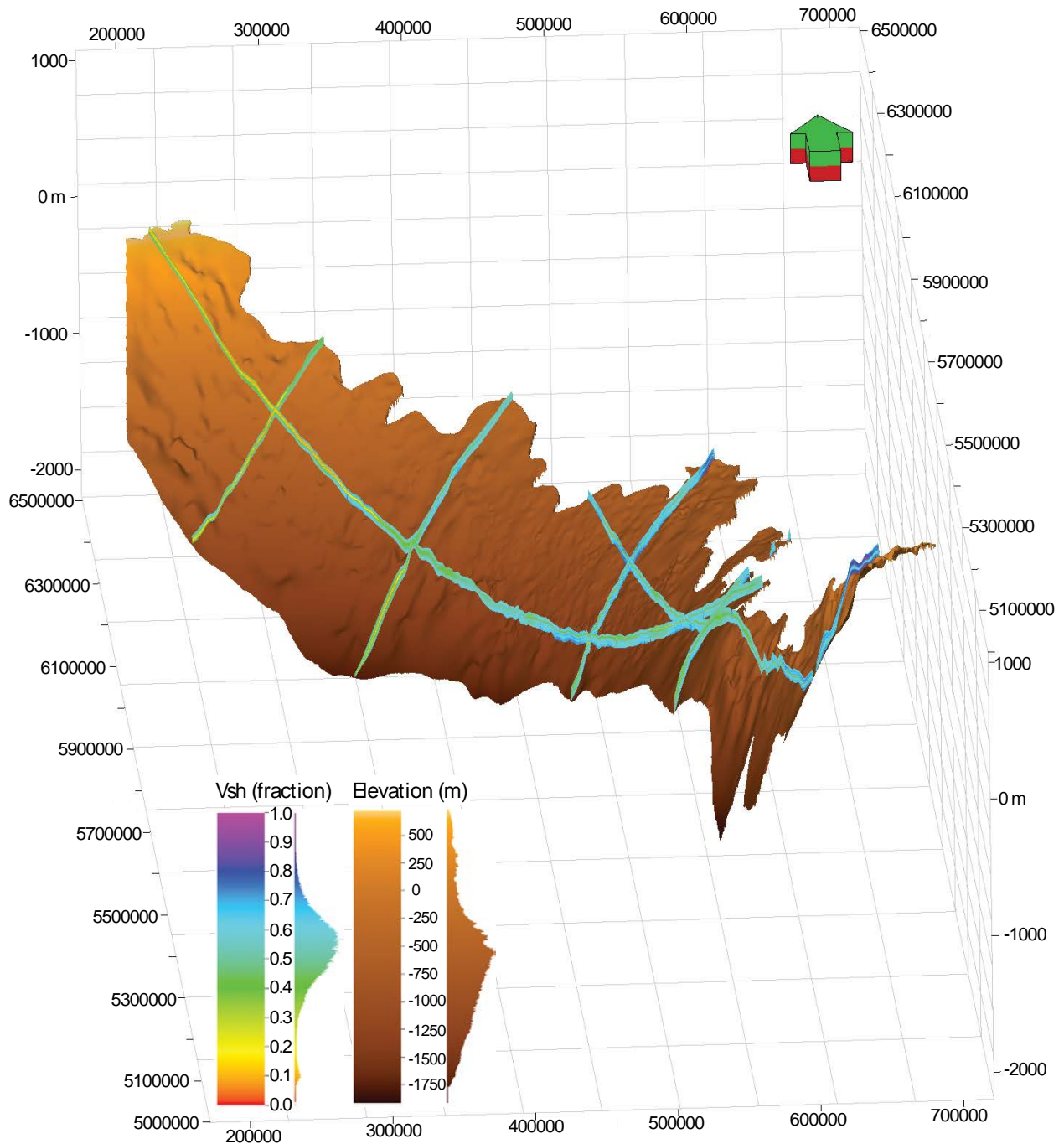


**Figure 12. Isometric views of the fence diagram of the kriged shale volume model. It shows that the sandstone abundance generally decreases from northwest to southeast. Locations of the cross-sections are indicated by lines 1 to 7 in [Figure 1](#). The surface at the base of the fences is the base of Cardium Formation. Vertical exaggeration is 100 times.**

[Figures 13](#) and [14](#) show isometric views of two simulated realizations of the density porosity model, the arithmetic mean of 100 realizations, and the kriged model. Each realization is different but equally probable and honours all of the data. The simulated realizations typically look “patchy” with a mixture of high and low values; however, the arithmetic mean of 100 realizations is smooth and nearly identical to a kriged model, with cell values tending towards the centre of the distribution ([Figure 14](#)).

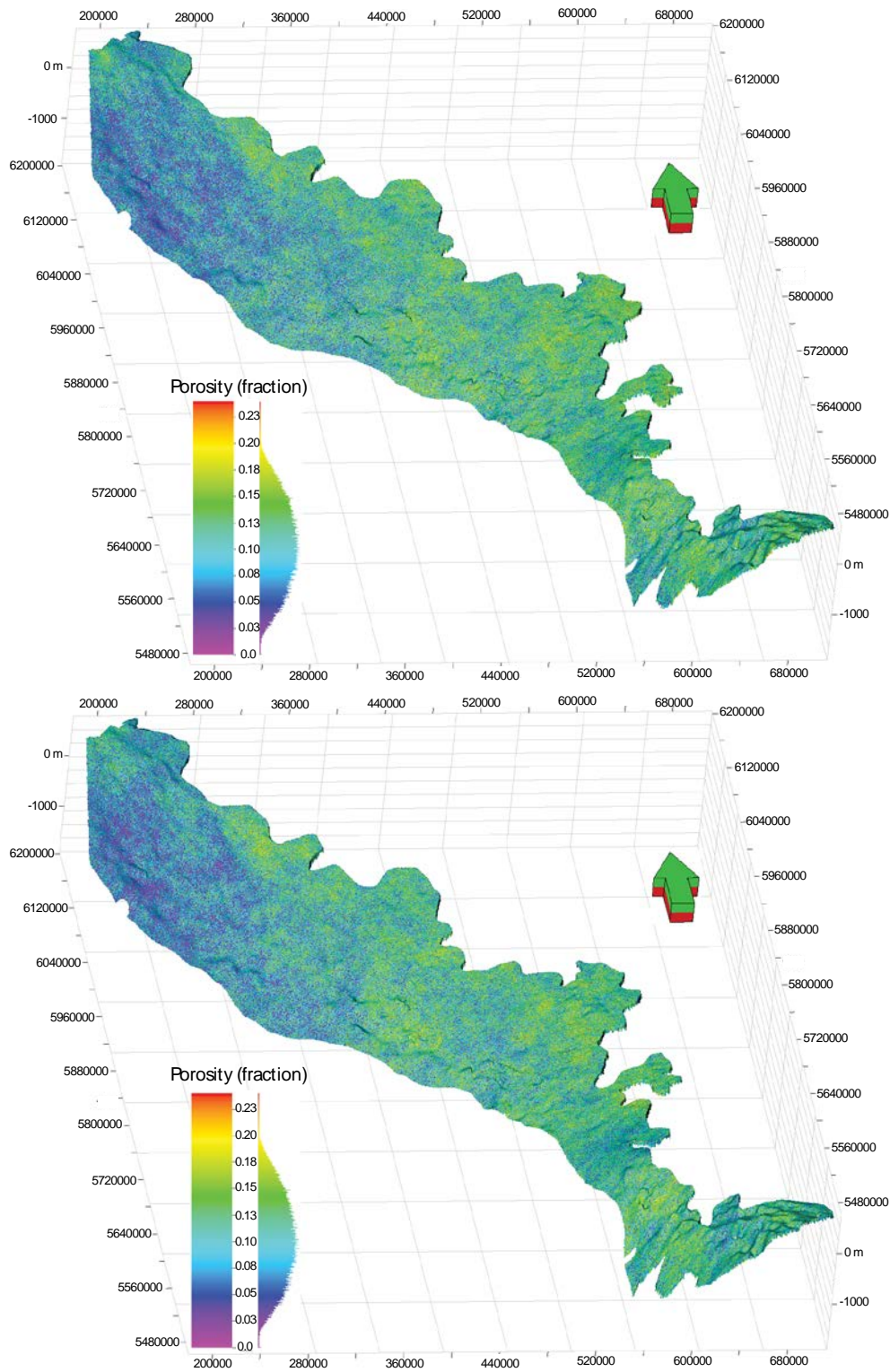


**Figure 13. Isometric view of two realizations for the density porosity model. Vertical exaggeration is 50 times.**

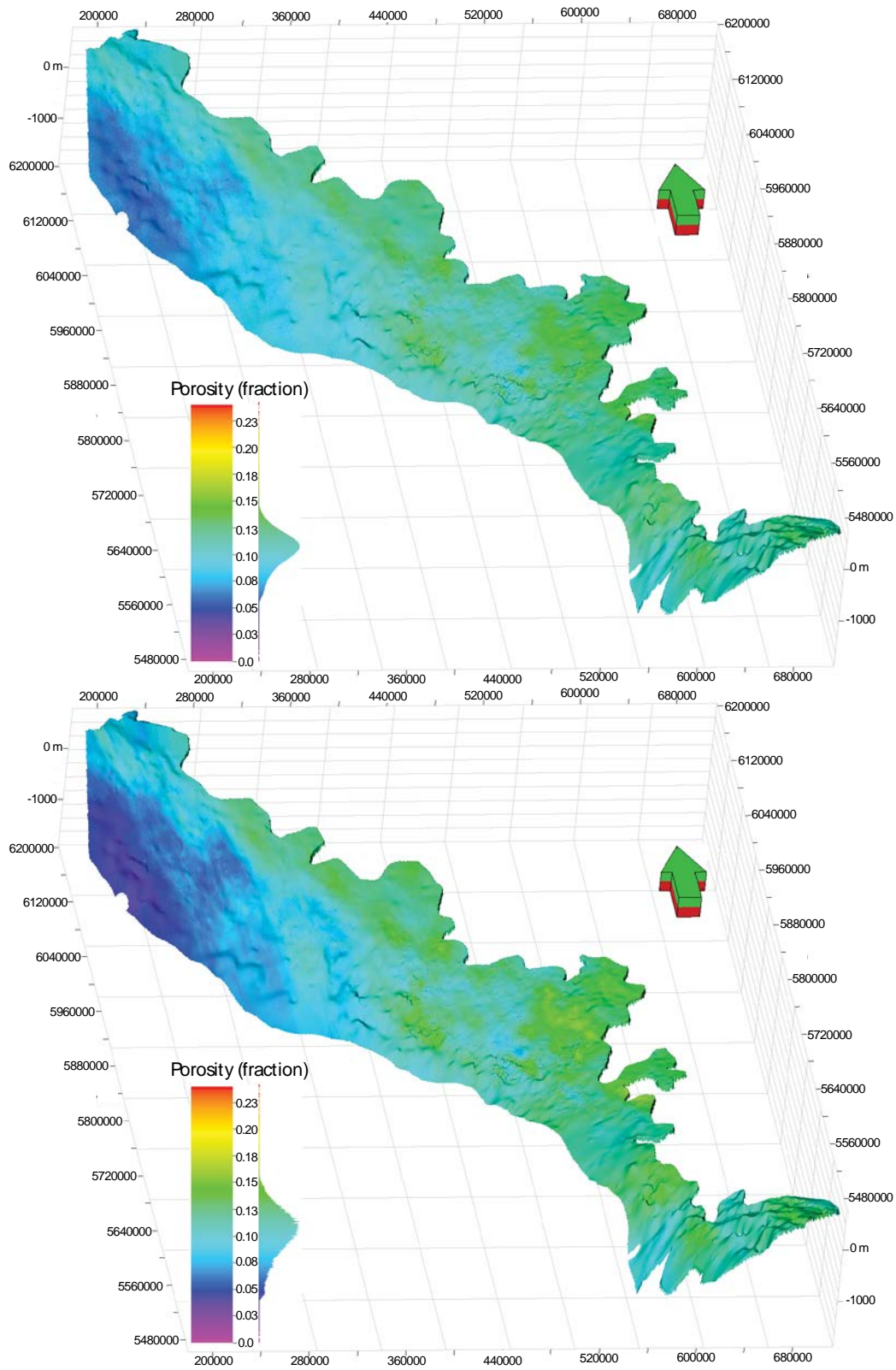


**Figure 14. Isometric view of the arithmetic mean of 100 realizations (top) and the kriging model (bottom) for the density porosity model. It shows that the total porosity generally increases from northwest to southeast. Vertical exaggeration is 50 times.**

Figure 15 shows isometric views of the 10<sup>th</sup> percentile (P10) and 90<sup>th</sup> percentile (P90) models of the density porosity and Figure 16 shows the fence diagram of the kriged model to show how it varies regionally throughout the model area.

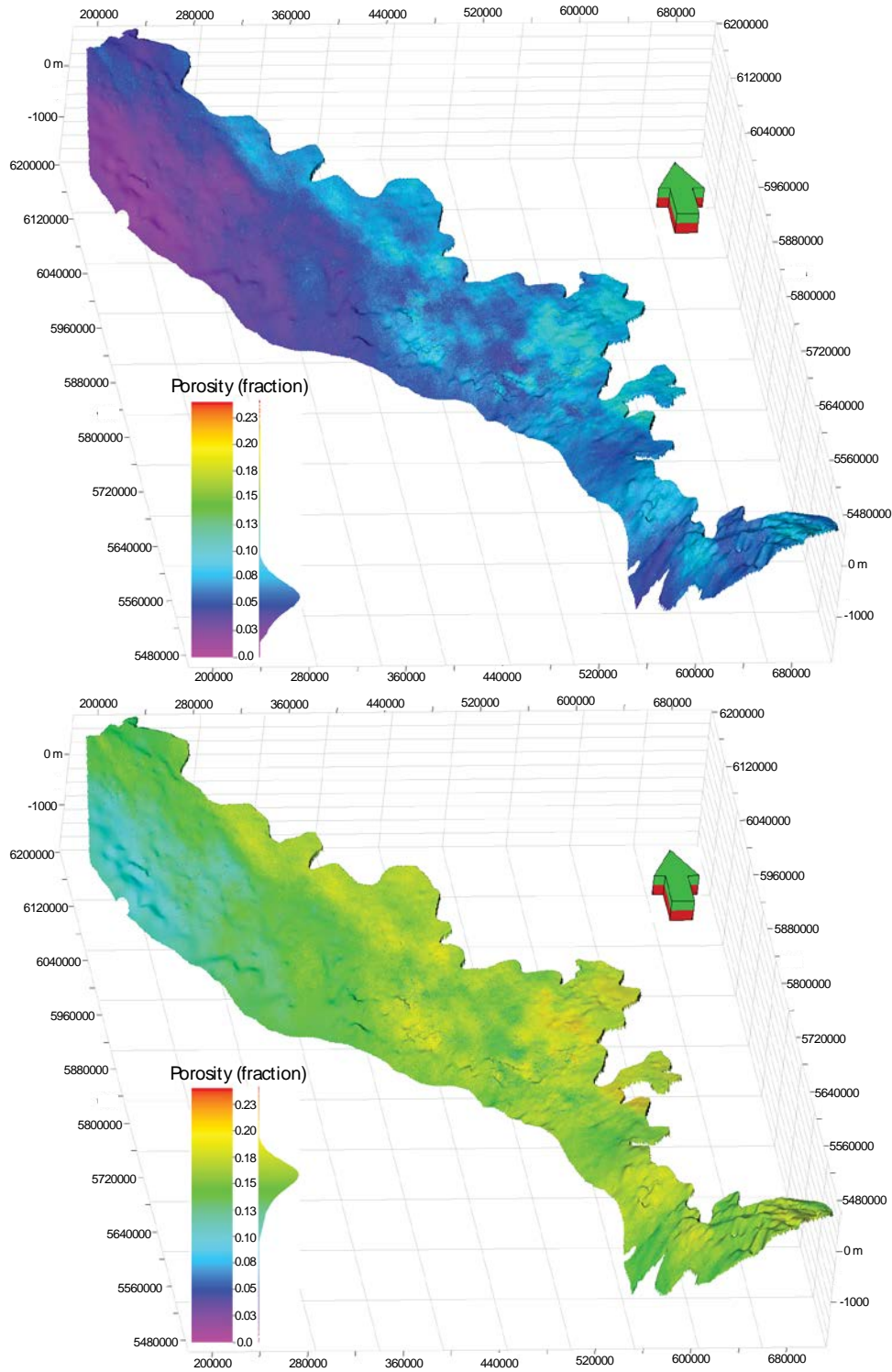
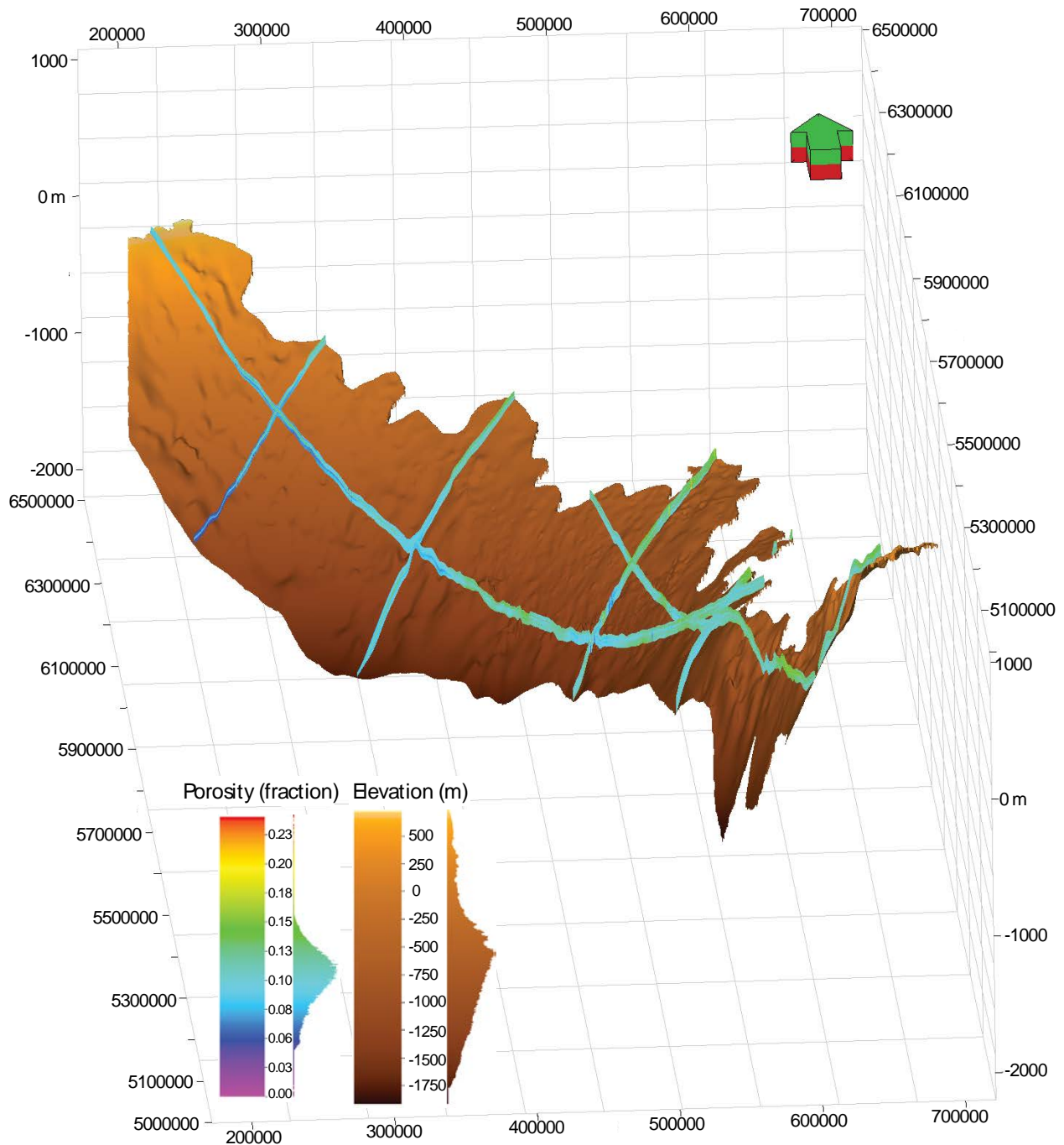
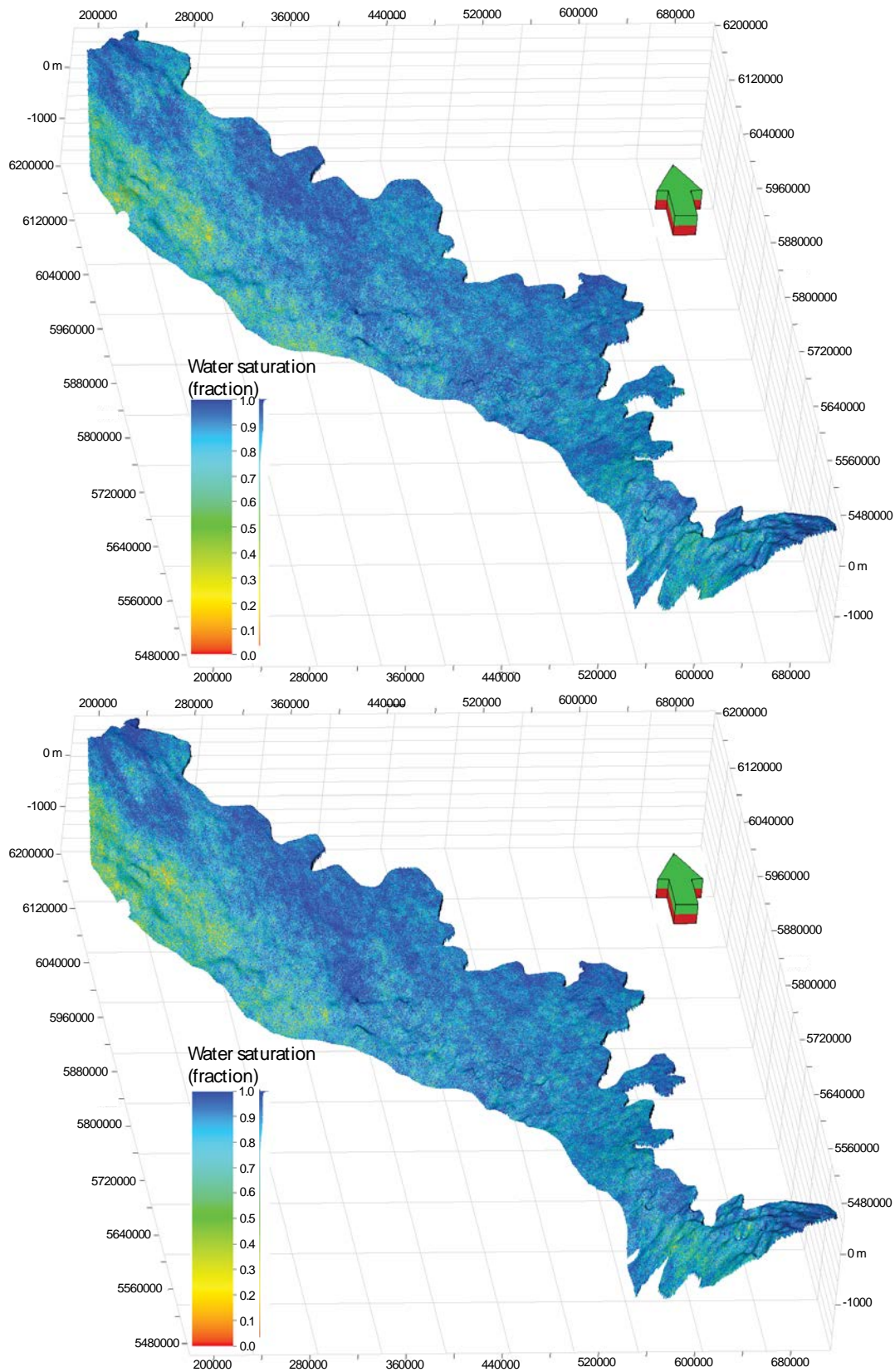


Figure 15. Isometric view of the 10<sup>th</sup> (top) and 90<sup>th</sup> (bottom) percentiles for the density porosity model. It shows that the total porosity generally increases from northwest to southeast. Vertical exaggeration is 50 times.



**Figure 16. Isometric view of the fence diagram for the density porosity model. It shows that the total porosity generally increases from northwest to southeast. Locations of the cross-sections are indicated by lines 1 to 7 in [Figure 1](#). The surface at the base of the fences is the base of Cardium Formation. Vertical exaggeration is 100 times.**

[Figures 17](#) and [18](#) show isometric views of two simulated realizations of the water saturation model, the arithmetic mean of 100 realizations, and the kriged model. Each realization is different but equally probable and honours all of the data. The simulated realizations typically look “patchy” with a mixture of high and low values; however, the arithmetic mean of 100 realizations is smooth and nearly identical to the kriged model, with cell values tending towards the centre of the distribution. [Figure 19](#) shows the fence diagram of the kriged model to show how it varies regionally throughout the model area.



**Figure 17. Isometric view of two realizations for the water saturation model. Vertical exaggeration is 50 times.**

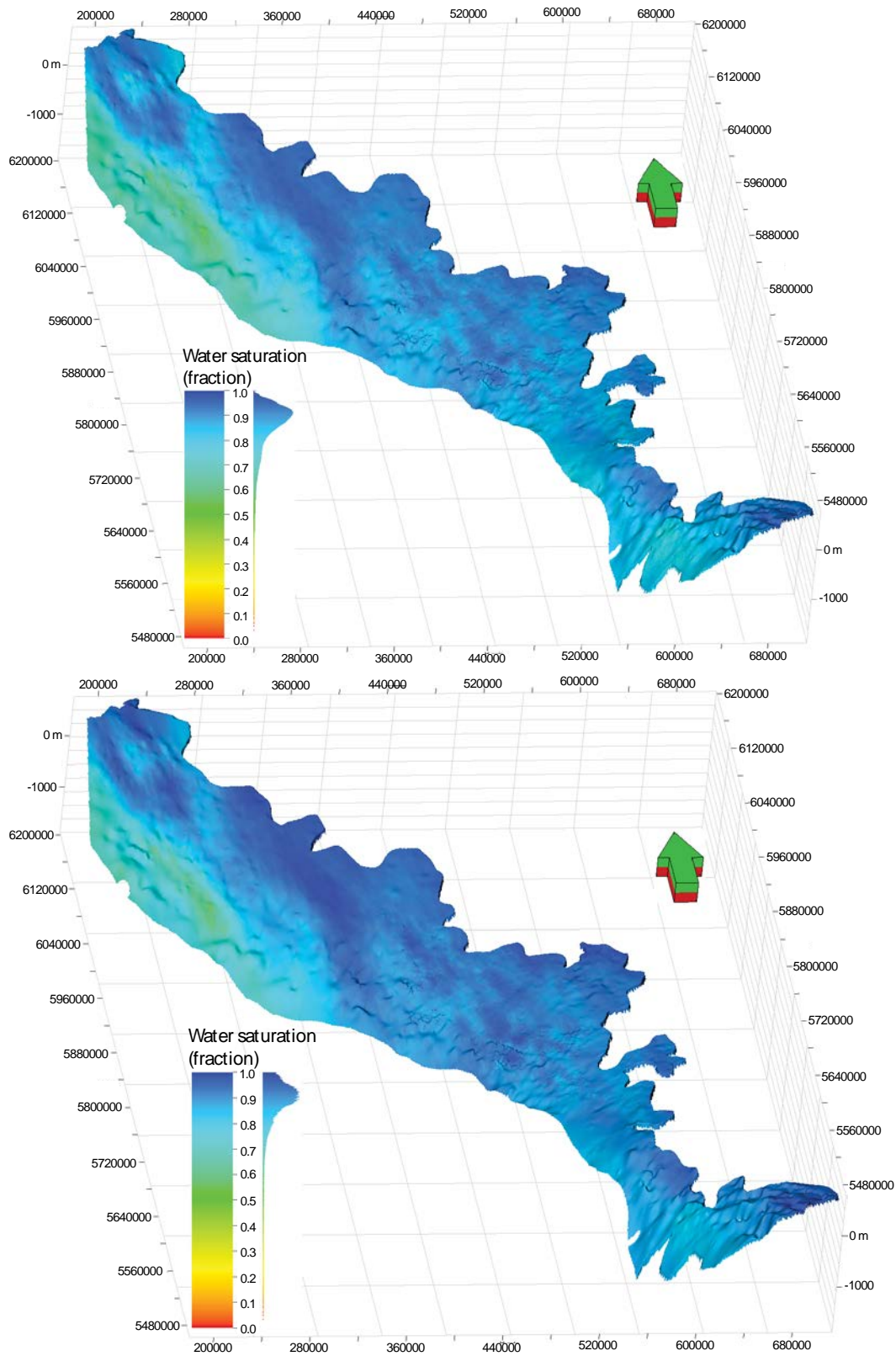


**Figure 18. Isometric view of the arithmetic mean of 100 realizations (top) and the kriging model (bottom) for the water saturation model. It shows that the water saturation generally increases from northwest to southeast. Vertical exaggeration is 50 times.**

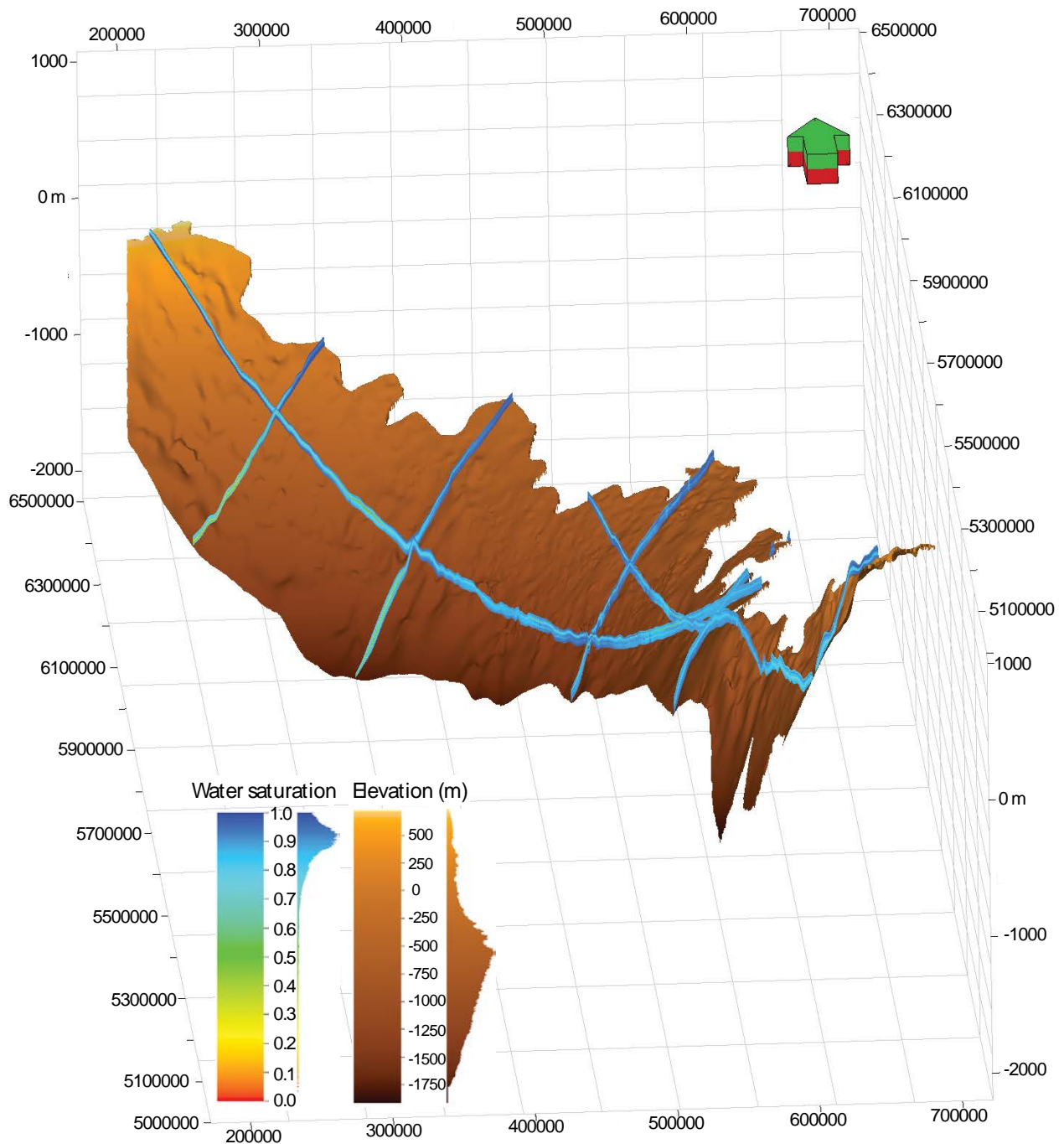


**Figure 19. Isometric views of the fence diagram of the kriged water saturation model. It shows that the water saturation generally increases from northwest to southeast. Locations of the cross-sections are indicated by lines 1 to 7 in [Figure 1](#). The surface at the base of the fences is the base of Cardium Formation. Vertical exaggeration is 100 times.**

## 6 Model Quality

The uncertainty of the 3D model is dependent on the quality of the input data, methods used, and decisions made during log analysis and 3D property modelling.

No normalization was applied to the gamma-ray logs and a single gamma-ray cutoff value of 15 API for the pure sandstone member and a single cutoff value of 140 API for the pure shale member were chosen and used across the entire region of the Cardium Formation in calculating the shale volume. The variation in the gamma-ray response to the pure sandstone and pure shale over such a large region will contribute to reducing the trueness to reality for the calculated shale volume or sandiness.

In calculating the porosity, a single grain density value of  $2.68 \text{ g/cm}^3$  and a single fluid density value of  $1 \text{ g/cm}^3$  were used across the entire Cardium Formation. This reduces the trueness to geological complexity and reality, although they were considered the most reasonable estimated values possible. A sensitivity analysis, obtained by taking the partial derivative of the response equation of density porosity with respect to matrix density and fluid density respectively, indicates that for a water-filled sandstone with a 30% porosity, an error of  $0.05 \text{ g/cm}^3$  in the assumed matrix density will only alter the calculated porosity by 2% porosity, and a variation of more than  $0.1 \text{ g/cm}^3$  in the fluid density corresponds to a similar 2% error in the calculated porosity. This is fortunate because a single estimated value for the matrix density and a single estimated value for the fluid density can still be helpful in revealing the regional trend of porosity.

The base and top of the Cardium Formation were adopted from 3D PGF v2 (Alberta Geological Survey, 2019) and the uncertainty associated with these surfaces will propagate into the modelling process and impact the quality of the 3D property model. In the construction of the model layers the Proportional option was used for the Cardium Formation and in property modelling the data used for interpolation was declustered by layer, meaning that neighbouring data points within the same layer as the point to be estimated were preferentially used. Having highly accurate geological surfaces ensures that the data points used for interpolation were from the rock deposited during the same time.

The uncertainty associated with the modelling was presented as the kriging standard deviation for each cell in the model, which was calculated from the 100 realizations from simulation. Figure 20 shows the uncertainty for the shale volume model, the density porosity model, and the water saturation model.

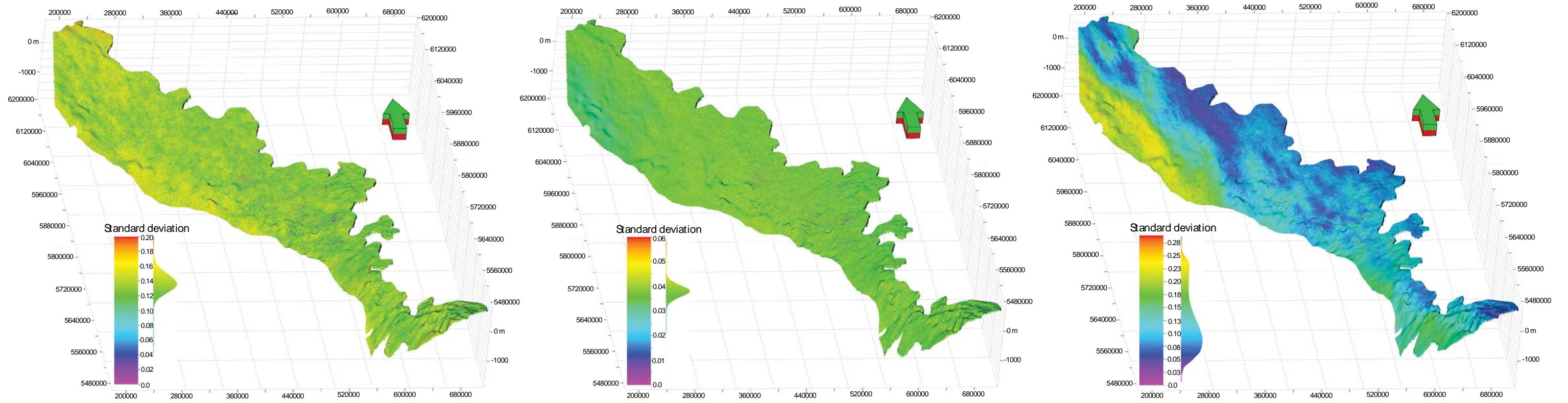


Figure 20. Isometric view of the kriging standard deviation for the shale volume model (left), the density porosity model (middle) and the water saturation model (right). Vertical exaggeration is 50 times.

Considering the uncertainties discussed above, the 3D property model developed for this study is appropriate only for regional-scale use (1:100 000). This model is not intended to be used in place of site-specific investigations because its accuracy is constrained by the data quality, quantity, distribution, and geological complexity at a regional scale.

## 7 Observations

The 3D property model illustrates the variation in sandstone abundance, porosity, and water saturation of the Cardium Formation in the subsurface of west-central and southwestern Alberta. Several regional trends are apparent from the 3D property model:

- The sandstone abundance generally decreases from northwest to southeast ([Figures 10 to 12](#)).
- In contrast to the sandstone abundance, the total porosity generally increases from northwest to southeast ([Figures 14 to 16](#)).
- The water saturation also generally increases from northwest to southeast ([Figures 18 and 19](#)).

The Cardium Formation is comprised of rocks ranging from mudstone to conglomerate. From the foothills in southwest towards the plains in northeast, the depositional environments of the Cardium Formation include coastal plain, estuarine, tidal, lagoonal, shoreface, and outer to inner shelf (Krause et al., 1994). In the subsurface of central Alberta, the Cardium Formation is represented by marine sediments and was subdivided into the Pembina River Member below and the Cardium Zone Member above (Krause and Nelson, 1984; Krause et al., 1987). The Pembina River Member consists of one or more coarsening-upward sequences that grade from shales to sandstones and then to variably thick conglomerates. The Cardium Zone Member also comprises coarsening-upward sequences, but in contrast to the Pembina River Member contains predominantly shales with lesser amounts of fine-grained sandstone and conglomerate (Krause et al., 1994). The middle Cardium Formation includes the upper Pembina River Member and its equivalent units; this interval contains significant estuarine, shoreface, and inner shelf sandstones, and conglomerates that accumulated in response to the lowering of relative sea level (Krause and Nelson, 1984; Keith, 1985, 1991; Krause et al., 1987; Joiner, 1991).

The sea level change trends are well revealed by the 3D property model. As mentioned previously, the model consists of 34 layers and each layer represents a slice of averagely ~2.5 m in thickness with the slice being numbered from bottom up. [Figures 21 to 25](#) show the 7<sup>th</sup>, 11<sup>th</sup>, 15<sup>th</sup>, 19<sup>th</sup>, and 23<sup>rd</sup> slices of the shale volume model, with the paleogeographic maps of Krause et al. (1994) for the lower, middle and upper Cardium Formation overlying on the 11<sup>th</sup>, 15<sup>th</sup>, 19<sup>th</sup> slices respectively. From the 7<sup>th</sup> slice to the 11<sup>th</sup> slice to the 15<sup>th</sup> slice it can be seen that a sand barrier is gradually developed in the northwest and the coastal line is moving from southwest to northeast, clearly indicating a lowering of relative sea level. In contrast, from the 15<sup>th</sup> slice to the 19<sup>th</sup> slice to the 23<sup>rd</sup> slice it can be seen that the coastal line is moving back from northeast to southwest, clearly indicating a relative sea level rise. These maps also confirm that the coastal plain has varied sandstone abundance, the shoreface and barriers have a relatively high sandstone percentage, and the shallow shelf and offshore have a relatively high shale volume.

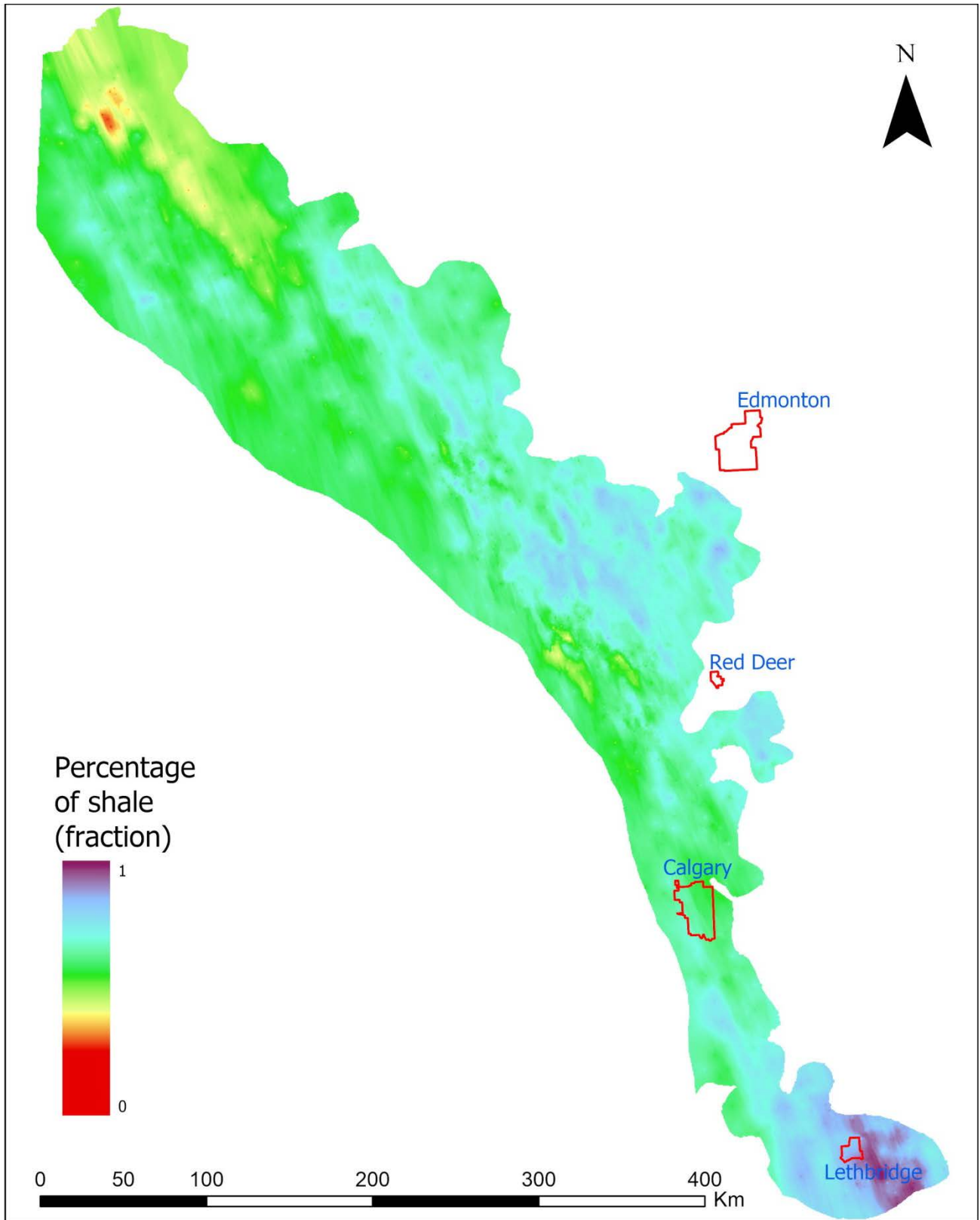


Figure 21. The 7<sup>th</sup> slice of the kriged shale volume model. It shows that a sand barrier started to emerge in the northwest.

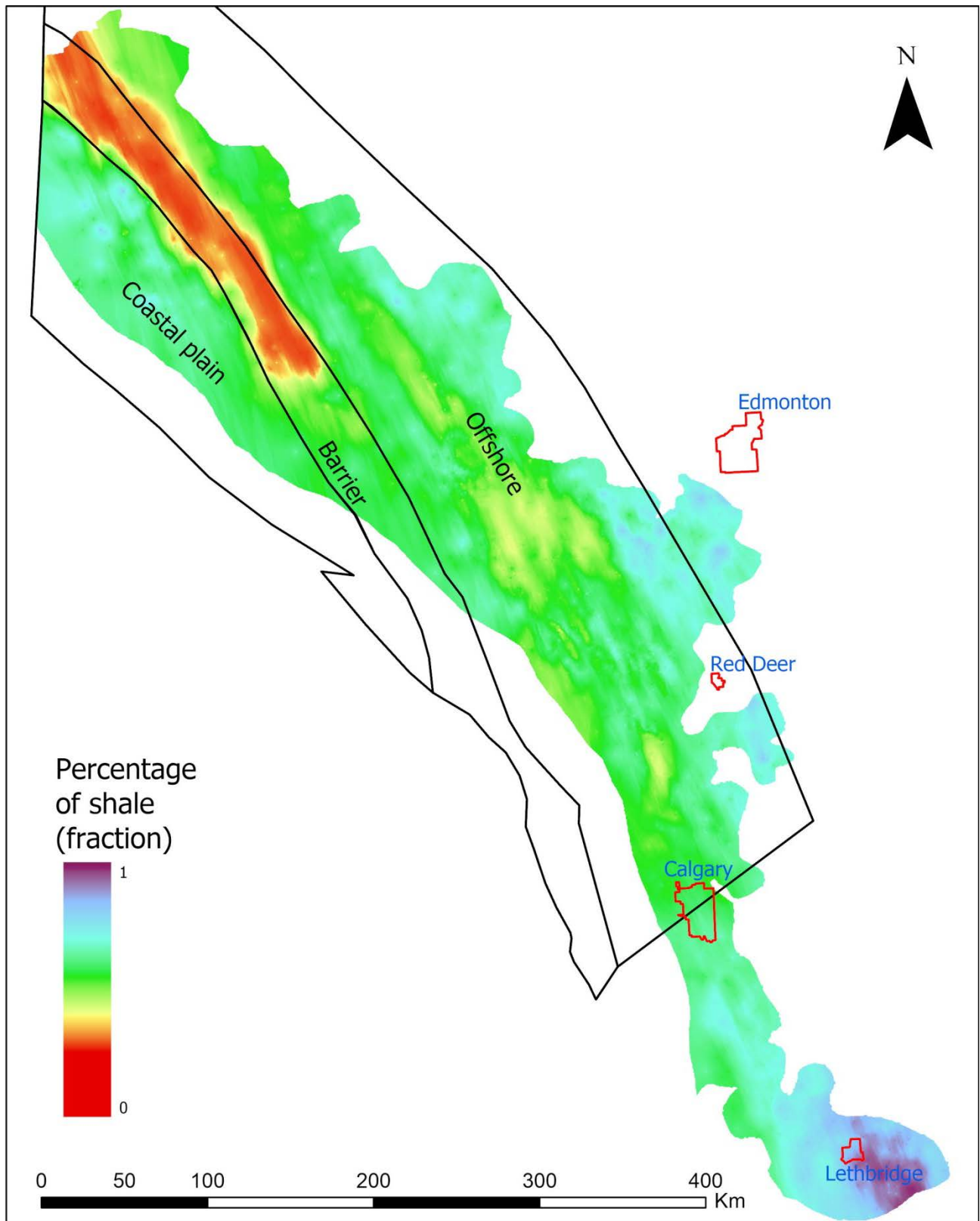


Figure 22. The 11<sup>th</sup> slice of the kriged shale volume model and the lower Cardium Formation paleogeographic map shown as black-line polygons (simplified from Krause et al., 1994).

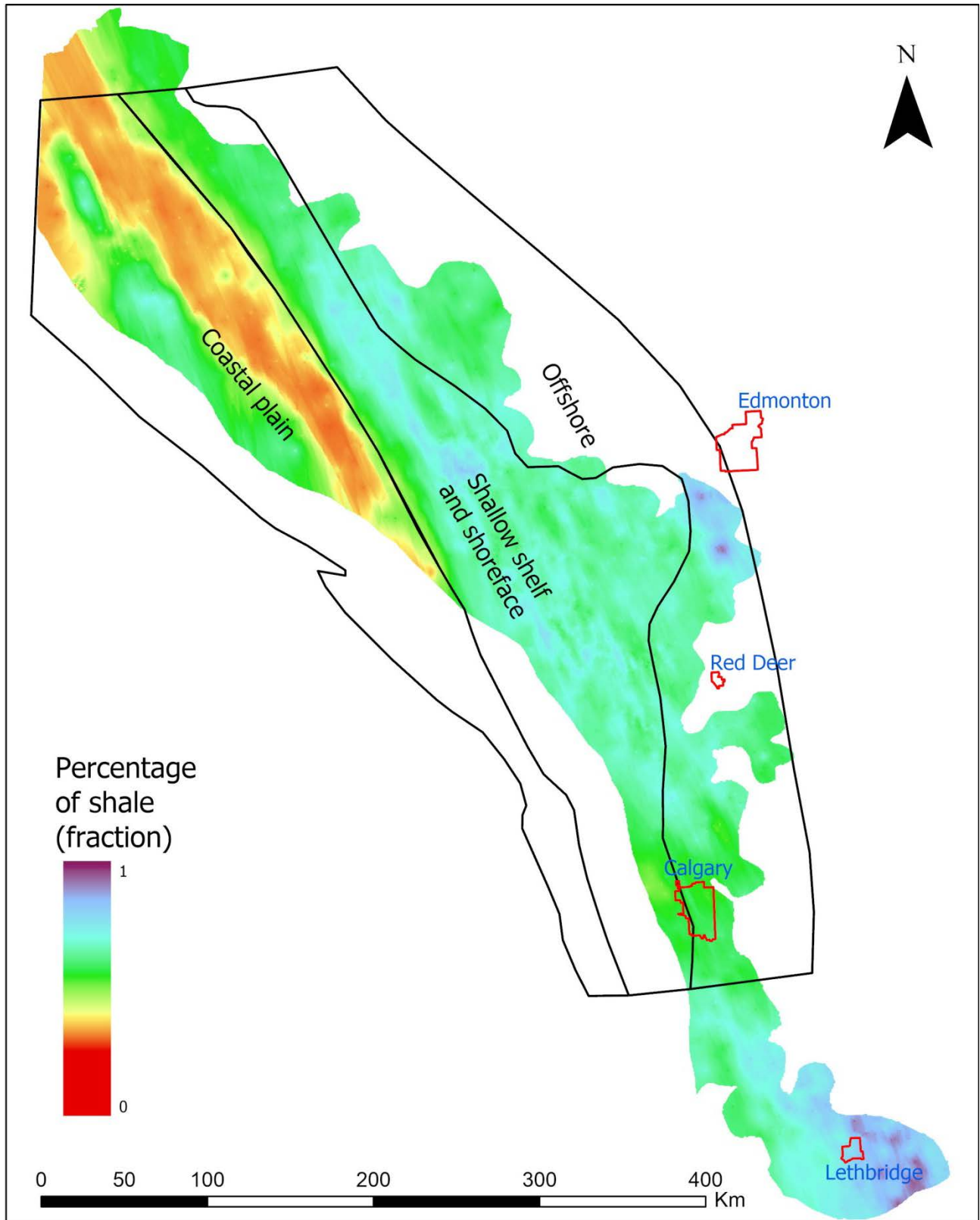


Figure 23. The 15<sup>th</sup> slice of the kriged shale volume model and the middle Cardium Formation paleogeographic map shown as black-line polygons (simplified from Krause et al., 1994).

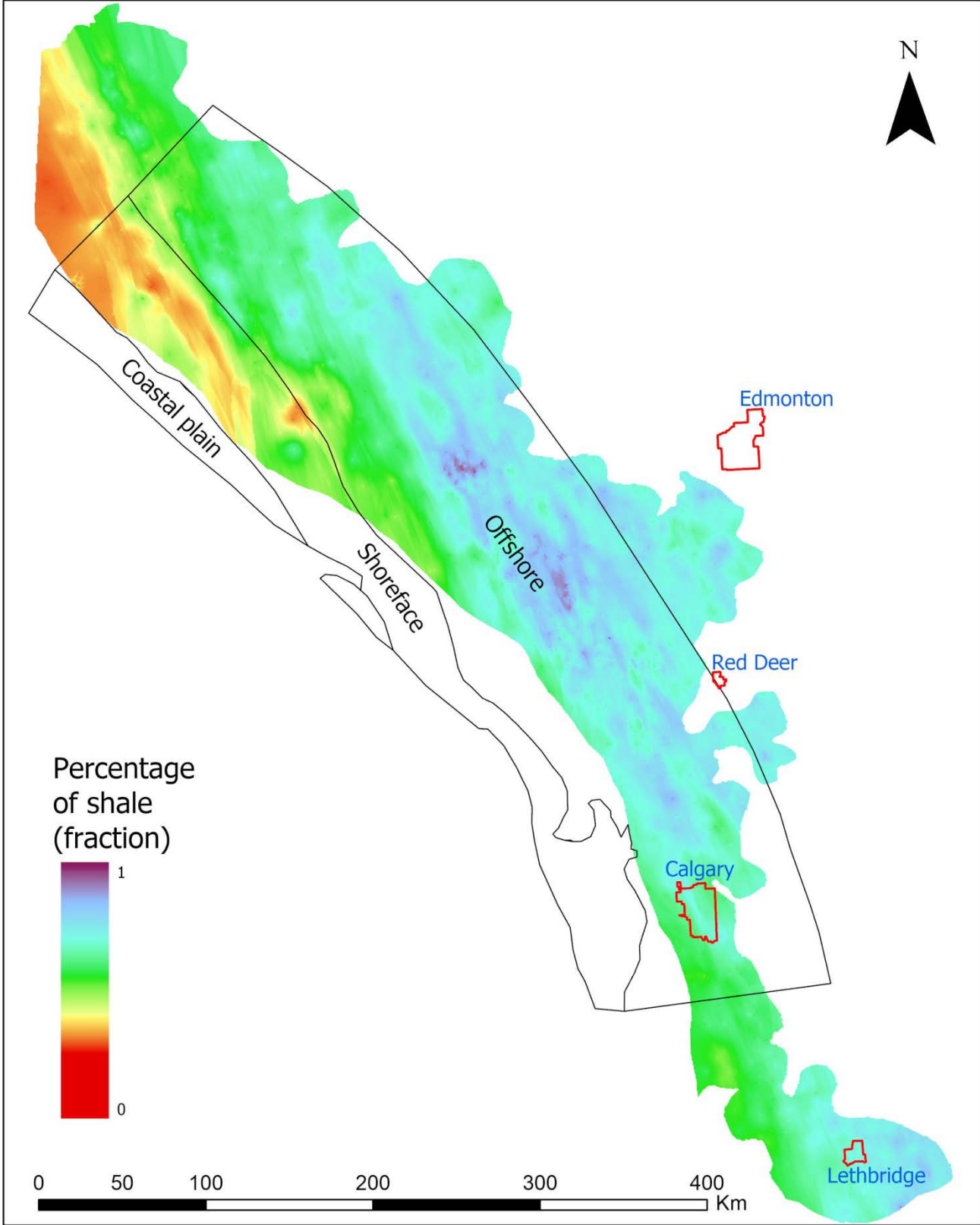


Figure 24. The 19<sup>th</sup> slice of the kriged shale volume model and the upper Cardium Formation paleogeographic map shown as black-line polygons (simplified from Krause et al., 1994).

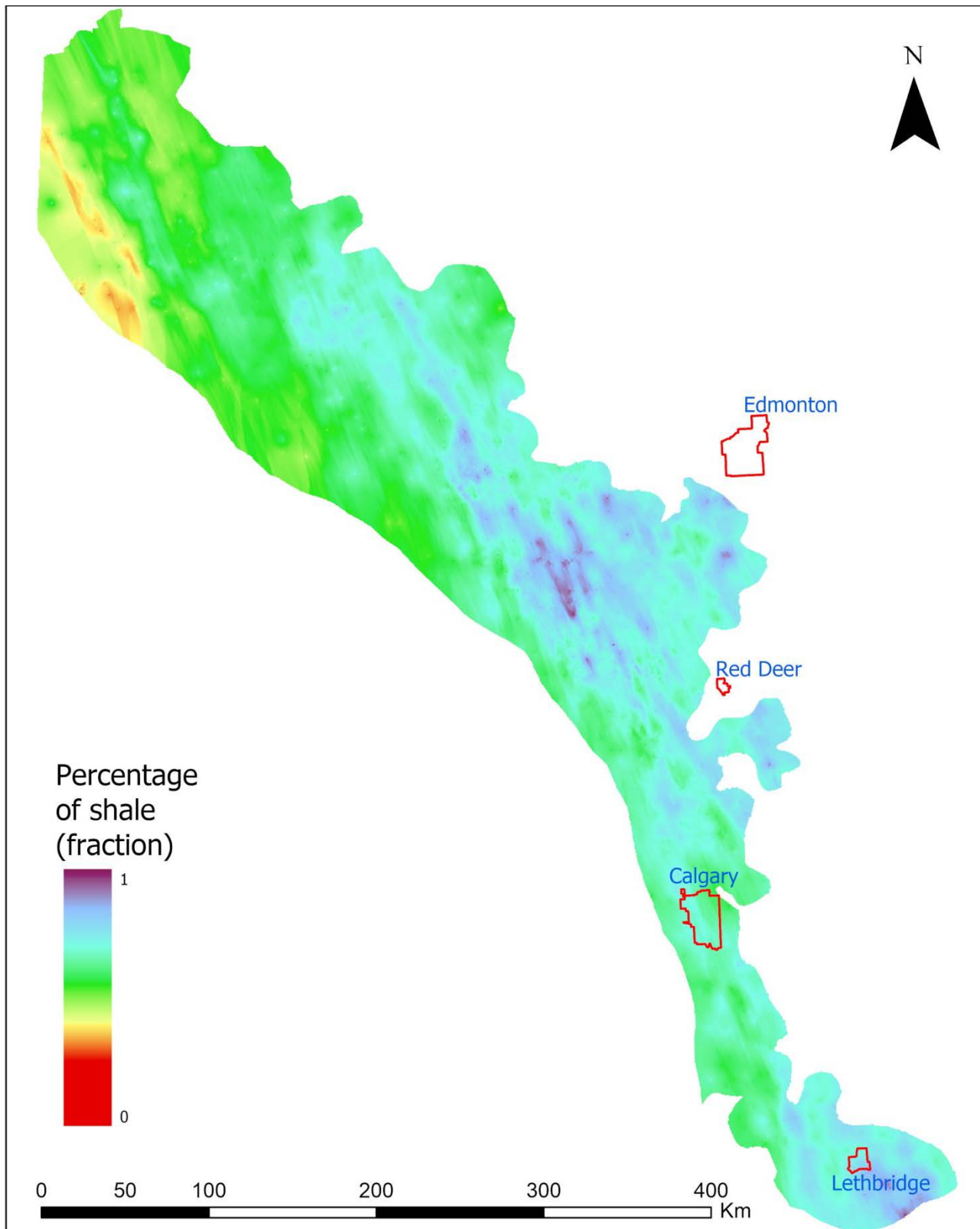


Figure 25. Comparison of the 23<sup>th</sup> slice of the kriged shale volume model.

The 3D property model also confirms the vertical lithological stacking pattern as mentioned previously, and the middle Cardium interval can be clearly seen in the cross-section of the model. In the cross-sections of the kriged shale volume model (Figures 26 and 27), the middle Cardium interval stands out clearly as a band of relatively high sandstone abundance (or low shale volume inversely) compared to the intervals above and below. In the cross-sections of the kriged density porosity model (Figure 28), the middle Cardium interval stands out as a band of relatively high porosity compared to the intervals above or below; however, this zone is not as clear as in the kriged shale volume model due to a greater variability in porosity. In the cross-sections of the kriged water saturation model (Figures 30 and 31), the middle Cardium interval stands out clearly as a band of relatively low water saturation compared to the intervals above and below. These observations explain why the middle Cardium Formation resulted in sandstone and conglomerate reservoirs in the supergiant Pembina Field, and the Willesden Green, Ferrier, Ricinus, Carrot Creek, and other smaller oil and gas fields.

The cross-sections of the 3D property model also reveal that the middle Cardium Formation is progradational from southwest to northeast (Figure 26, lower; Figure 30, lower). The cross-sections of the kriged density porosity model also reveal some details of the coarsening-upward parasequences for the Cardium Formation (Figures 28 and 29).

It is noteworthy that the shale volume variable and the density porosity variable do not appear to correlate well in some intervals and area (compare Figure 26 with Figure 28, and Figure 27 with Figure 29). Qualitative thin-section analyses for the Paleogene Paskapoo sandstones by Hughes et al. (2017) indicated that for sandstone units with similar grain size, a wide range in porosity values can arise owing to the amount of cementation and other pore-filling processes. Hughes et al. (2017) interpreted the disparity between hydraulic properties of the sandstone units of the Paskapoo Formation by hypothesizing that the porosity of the sandstones is governed by cementation rather than grain size. Although the findings of Hughes et al. (2017) are concerned with the Paleogene Paskapoo Formation, they may help to explain the low correlation between the shale volume variable and the density porosity variable in some parts of the Cardium Formation. However, further detailed study is needed to understand the complex relationships among the lithology, diagenesis, and porosity in the Cardium Formation.

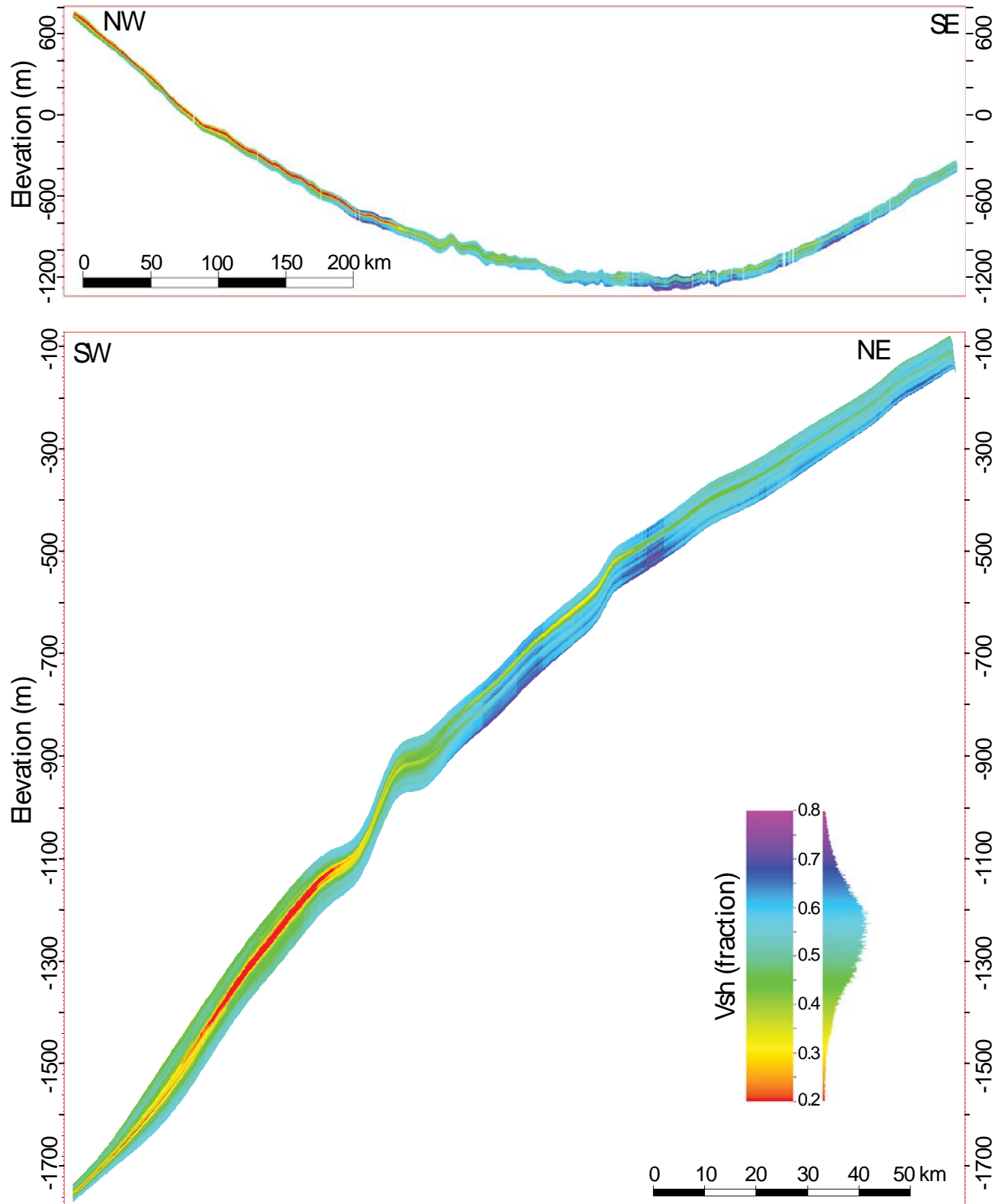


Figure 26. Cross-sections of the kriged shale volume model. The middle Cardium interval stands out as a band of relatively high sandstone abundance in red and yellow. Location of the cross-section is indicated by line 6 (upper) and line 2 (lower) in [Figure 1](#). Vertical exaggeration is 100 times.

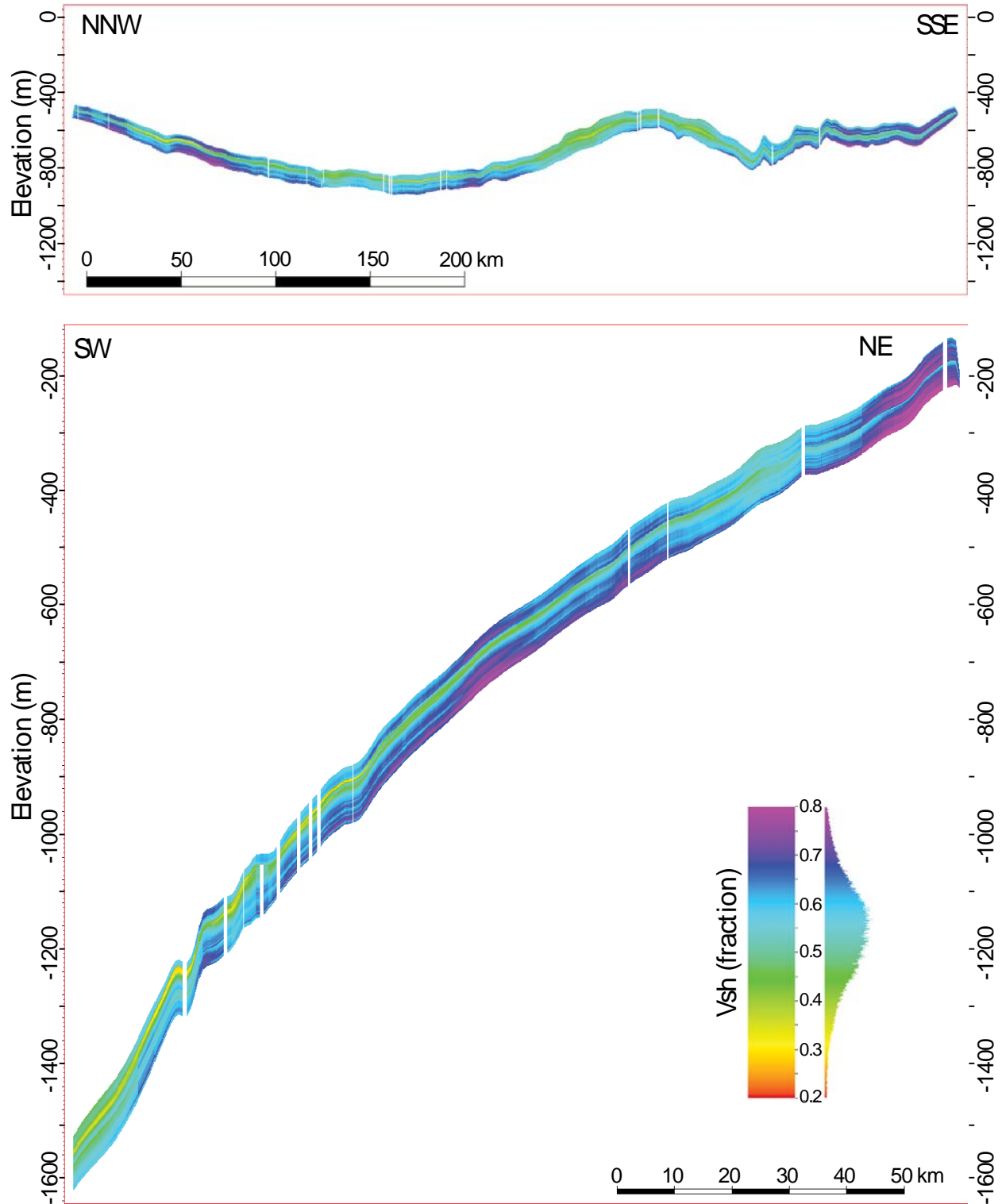


Figure 27. Cross-sections of the kriged shale volume model. The middle Cardium interval stands out as a band of relatively high sandstone abundance in yellow, green and cyan. Location of the cross-section is indicated by line 7 (upper) and line 3 (lower) in [Figure 1](#). Vertical exaggeration is 100 times.

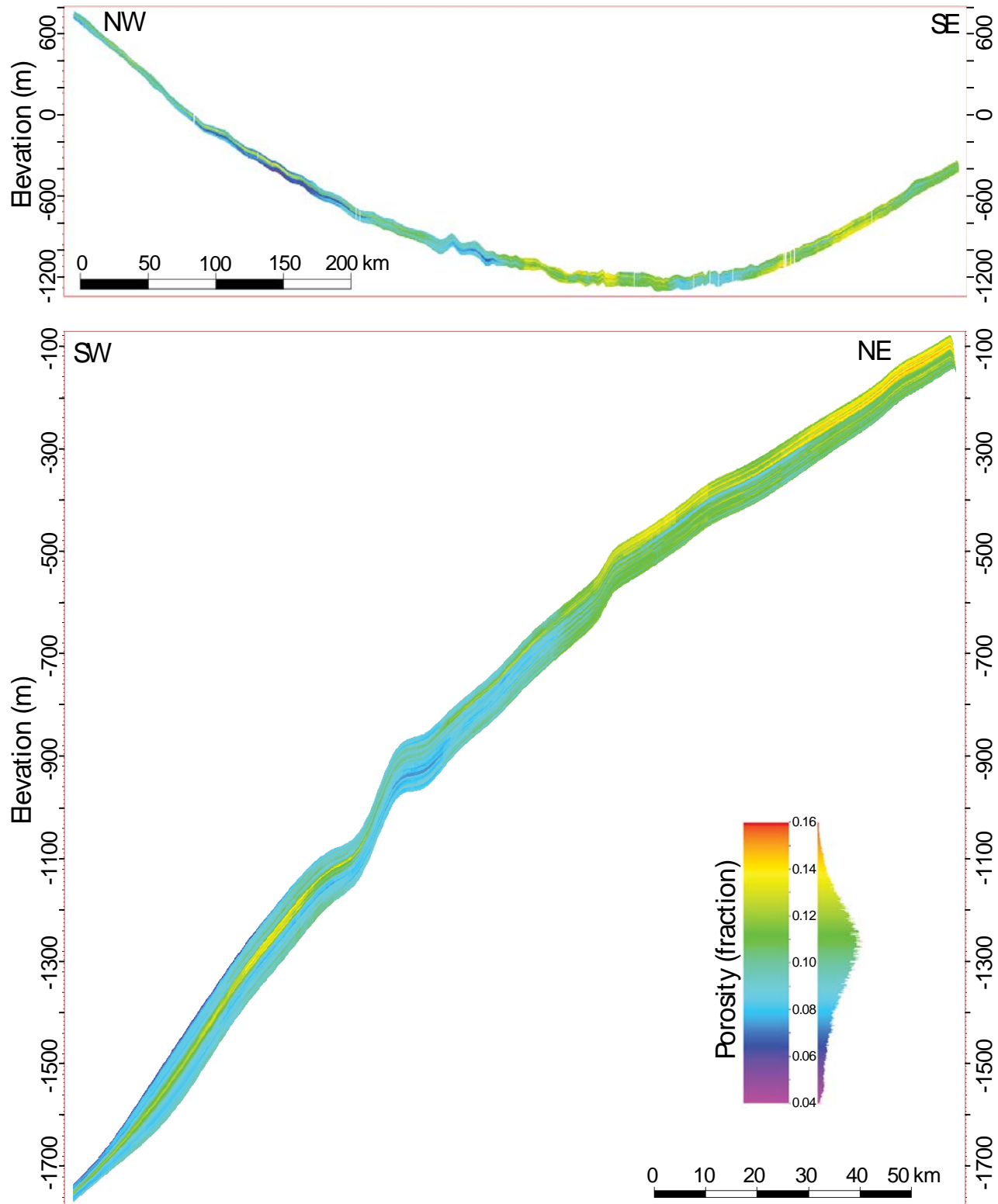


Figure 28. Cross-sections of the kriged density porosity model. The middle Cardium interval stands out as a band of relatively high porosity in yellow in the west. Location of the cross-section is indicated by line 6 (upper) and line 2 (lower) in [Figure 1](#). Vertical exaggeration is 100 times.

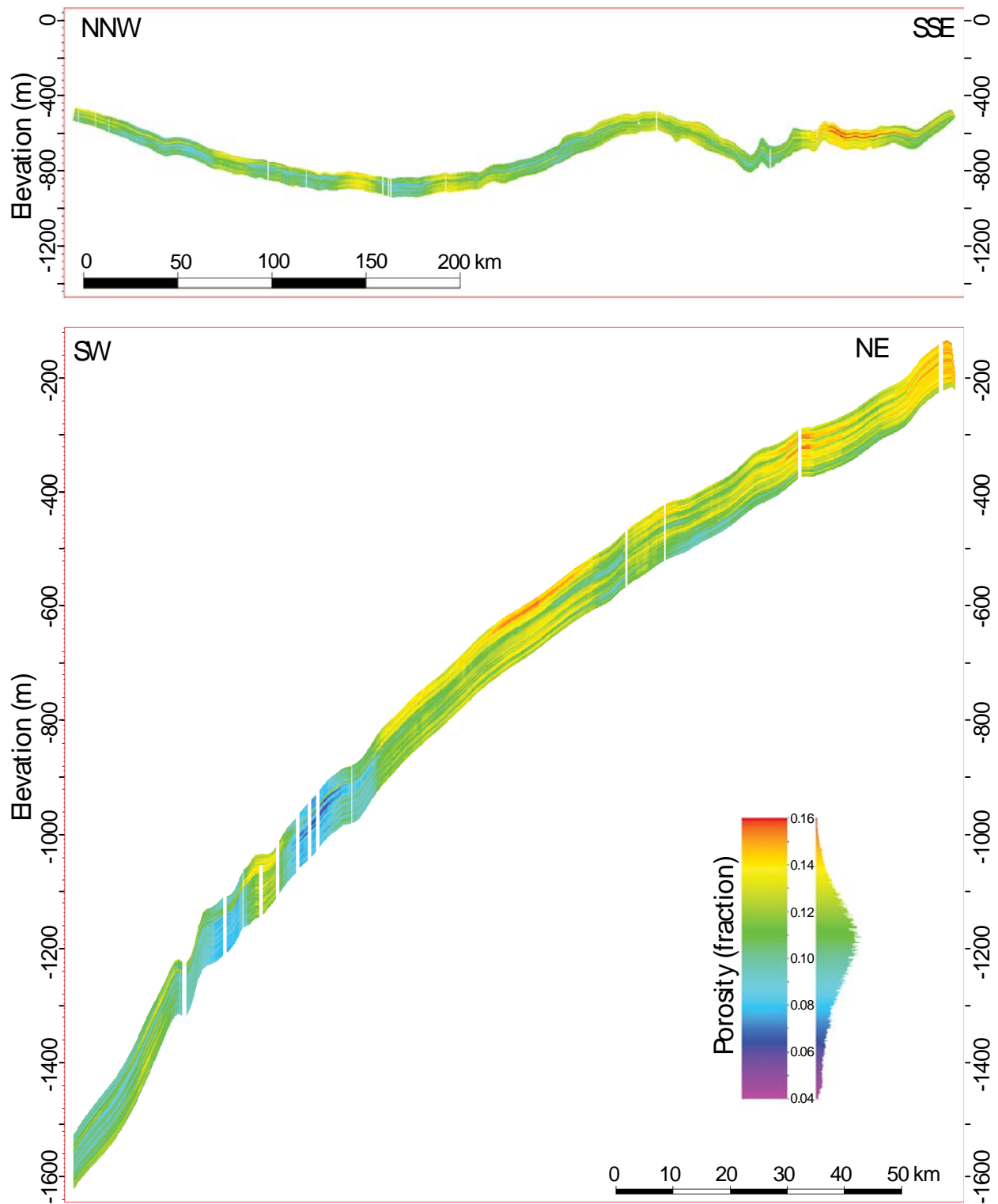


Figure 29. Cross-sections of the kriged density porosity model. Location of the cross-section is indicated by line 7 (upper) and line 3 (lower) in [Figure 1](#). Vertical exaggeration is 100 times.

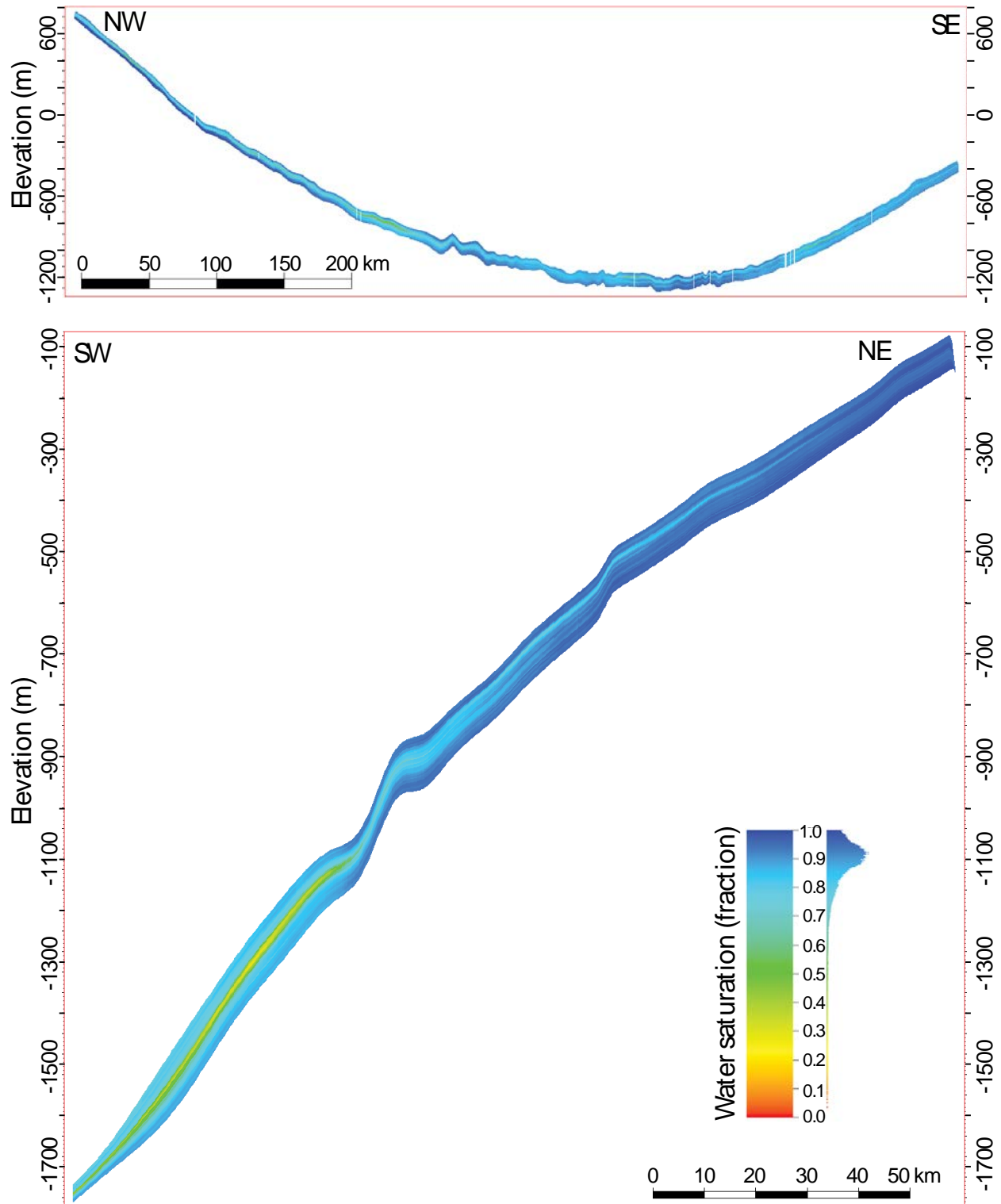


Figure 30. Cross-sections of the kriged water saturation model. The middle Cardium interval stands out as a band of relatively low water saturation in yellow, green and cyan. Location of the cross-section is indicated by line 6 (upper) and line 2 (lower) in [Figure 1](#). Vertical exaggeration is 100 times.

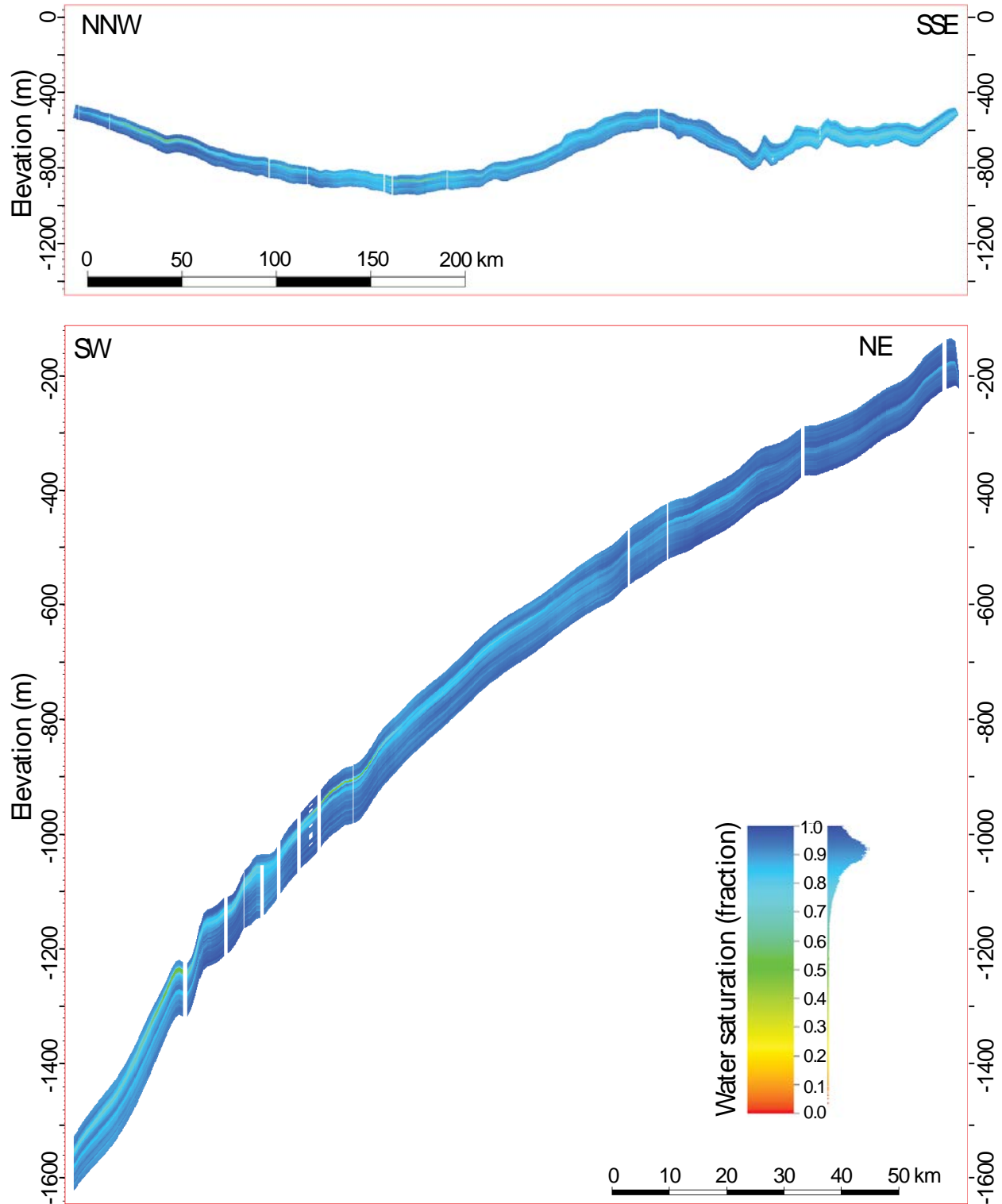


Figure 31. Cross-sections of the kriged water saturation model. The middle Cardium interval stands out as a band of relatively low water saturation in cyan. Location of the cross-section is indicated by line 7 (upper) and line 3 (lower) in [Figure 1](#). Vertical exaggeration is 100 times.

## 8 Model Outputs

There are digital data model outputs deconstructed from the Cardium 3D property model available in standard formats on the website of the Alberta Geological Survey ([https://ags.aer.ca/data-maps-models/MOD\\_2020\\_01.html](https://ags.aer.ca/data-maps-models/MOD_2020_01.html); Mei and Berhane, 2020):

**Model extents:** zone model extents published as GIS data polygon features.

**Model horizons:** horizons published as gridded data in ASCII format.

**Model properties:** populated model property of shale volume, porosity, and water saturation (mean of 100 realizations and standard deviation) as point data in ASCII format and Petrel format.

## 9 Summary Remarks

The 3D property model developed for this study illustrates the degree of heterogeneity of shale volume, porosity, and water saturation in the Cardium Formation at a higher resolution compared to previous studies. It helps reveal depositional environments, history, and stacking patterns and provides insight to vertical and lateral connectivity of sandstone units and the degree of confinement (or compartmentalization) of the surrounding mudstone. Knowledge of sandstone unit geometry is useful for identifying localized reservoirs assuming that the sandiness value, in terms of shale volume inversely, is a proxy for permeability. However, given the uncertainty in the data used and the large area of the study, the 3D property model is appropriate only for regional-scale use (1:100 000) and not intended for use in place of site-specific investigations.

## 10 References

- Alberta Geological Survey (2015): Alberta Table of Formations; Alberta Energy Regulator, URL <<https://ags.aer.ca/activities/table-of-formation.htm>> [Accessed on August 22, 2018].
- Alberta Geological Survey (2019): 3D provincial geological framework model of Alberta, version 2; Alberta Energy Regulator / Alberta Geological Survey, AER/AGS Model 2018-02.
- Braunberger, W. F. and Hall, R. L. (2001a): Ammonoid faunas from the Cardium Formation (Turonian-Coniacian, Upper Cretaceous) and contiguous units, Alberta, Canada; I, Scaphitidae; Canadian Journal of Earth Sciences, v. 38, p. 333–346.
- Braunberger, W. F. and Hall, R. L. (2001b): Ammonoid faunas from the Cardium Formation (Turonian-Coniacian; Upper Cretaceous) and contiguous units, Alberta, Canada; II, Collignoniceratidae and Placenticeratidae; Canadian Journal of Earth Sciences, v. 38, p. 1117–1128.
- Caldwell, W.G.E. (1984): Early Cretaceous transgressions and regressions in the southern Interior Plains; *in* The Mesozoic of Middle North America, D.F. Stott and D.J. Glass (eds.), Canadian Society of Petroleum Geologists Memoir 9, p. 173–203.
- Canadian Well Logging Society (2002) [electronic resource]: Water resistivity catalogue: Rw maps and data for Western Canadian sedimentary basin and North Dakota, northern territories, East Coast.
- Clarkson, C. R. and Pedersen, P. K. (2011): Production analysis of western Canadian unconventional light oil plays; Canadian Unconventional Resources Conference, Calgary, Alberta, Canada, 22 p.
- Crain, E.R. (1986): The Log Analysis Handbook Volume 1: Quantitative Log Analysis Methods. PennWell Publishing Company, Tulsa, Oklahoma, p. 214–215.
- Daly, C., Quental, S. and Novak, D. (2010): A faster, more accurate Gaussian simulation; GeoCanada Conference, Calgary, AB, Canada, p. 10–14.
- Hall, R. L., Krause, F. F., Joiner, S. D. and Deutsch, K. B. (1994): Biostratigraphic evaluation of a sequence stratigraphic bounding surface: the Cardinal/Leyland unconformity (“E5/T5 surface”) in the Cardium Formation (Upper Cretaceous; Upper Turonian-lower Coniacian) at Seebe, Alberta; Bulletin of Canadian Petroleum Geology, v. 42, no. 3, p. 296–311.
- Haq, B.U., Hardenbol, J., and Vail, P.R. (1987): Chronology of fluctuating sea levels since the Triassic; Science, v. 235, p. 1156–1166.
- Hart, B.S and Plint, A. G. (1993): Origin of an erosion surface in shoreface sandstones of the Kakwa Member (Upper Cretaceous Cardium Formation, Canada): importance for reconstruction of stratal geometry and depositional history; International Association of Sedimentologists Special Publication 18, p. 451–467.
- Hart, B.S. and Plint, A. G. (2003): Stratigraphy and sedimentology of shoreface and fluvial conglomerates: insights from the Cardium Formation in NW Alberta and adjacent British Columbia; Bulletin of Canadian Petroleum Geology v. 451, p. 437–464.
- Hughes, A.T., Smerdon, B.D. and Alessi, D.S. (2017): A summary of hydraulic conductivity values for the Paskapoo Formation in west-central Alberta; Alberta Energy Regulator, AER/AGS Open File Report 2016-03, 25 p.
- Joiner, S.D. (1991): Stratigraphic architecture of a parasequence set and the genetic implications for the Cardium Fm. at Pembina; M.Sc. thesis, The University of Calgary, 384 p.
- Keith, D.A.W. (1985): Sedimentology of the Cardium Formation (Upper Cretaceous), Willesden Green Field, Alberta; M.Sc. thesis, McMaster University, 241 p.

- Keith, D.A.W. (1991): Sedimentology and geometry of the Cardium (Turonian) sandstone and conglomerate at Willesden Green Field, Alberta: Offshore sand body or incised prograding strand plain deposit? *in* Shelf Sand and Sandstone Bodies: Geometry, Facies and Sequence Stratigraphy, D.J.P. Swift, G.F. Oertel, R.W. Tillman, and J.A. Thorne (eds.), International Association of Sedimentologists, Special Publication 14, p. 457–486.
- Klein, M., Kenealey, G. and Makowecki, B. (2012): Comparison of hydraulic fracture fluids in multi-stage fracture stimulated horizontal wells in the Pembina Cardium Formation; Paper presented at the Society of Petroleum Engineers Hydrocarbon Economics and Evaluation Symposium, Calgary, Alberta, 20 p.
- Krasey, R. (1985): A first-look method for analyzing mature waterfloods; *Journal of Canadian Petroleum Technology*, v. 24, p. 68–75.
- Krause, F. F., and Braunberger, W. F. (2016): COMMENT: Interregional correlation of unconformities in Upper Cretaceous strata, Western Interior Seaway: Biostratigraphic and sequence-stratigraphic evidence for eustatic change; *Geological Society of America Bulletin*, v. 128, no. 5/6, p. 1044–1052.
- Krause, F.F. and Nelson, D.A. (1984): Storm event sedimentation: Lithofacies association in the Cardium Formation, Pembina area, west-central Alberta, Canada; *in* The Mesozoic of Middle North America, D.F. Stott and D.J. Glass (eds.), Canadian Society of Petroleum Geologists, Memoir 9, p. 485–511.
- Krause, F.F., Collins, H.N., Nelson, D.A., Macheimer, S.D., and French, P.R. (1987): Multiscale anatomy of a reservoir: Geological characterization of Pembina-Cardium pool, west-central Alberta, Canada; *American Association of Petroleum Geologists Bulletin*, v. 71, p. 1233–1260.
- Krause, F. F., Deutsch, K. B., Joiner, S. D., Barclay, J. E., Hall, R. L., and Hills, L. V. (1994): Cretaceous Cardium Formation of the Western Canada Sedimentary Basin; *in* Geological Atlas of the Western Canada Sedimentary Basin, G. D. Mossop and I. Shetsen (eds.), Canadian Society of Petroleum Geologists and Alberta Research Council, p. 375–385.
- Krause, F.F., Hall, R.L., Joiner, S.D. and Deutsch, K.B. (1995): Biostratigraphic evaluation of sequence stratigraphic bounding surface: the Cardinal/Leyland unconformity ("E5/T5 surface") in the Cardium Formation (Upper Cretaceous; upper Turonian - lower Coniacian) at Seebe, Alberta: Reply; *Bulletin of Canadian Petroleum Geology*, v. 43, p. 347–355.
- Lambeck, K., Cloetingh, S., and McQueen, H. (1987): Intraplate stress and apparent changes in sea level: the basins of northwestern Europe; *in* Sedimentary Basins and Basin-forming Mechanisms, C. Beaumont and A.J. Tankard (eds.), Canadian Society of Petroleum Geologists, Memoir 12, p. 259–268.
- Mei, S. and Berhane, M. (2020): Three-dimensional property model of the Upper Cretaceous Cardium Formation in west-central and southern Alberta (dataset, multiple files); Alberta Energy Regulator / Alberta Geological Survey, AER/AGS Model 2020-01, URL <[https://ags.aer.ca/data-maps-models/MOD\\_2020\\_01.html](https://ags.aer.ca/data-maps-models/MOD_2020_01.html)>.
- Nielsen, A.R. and Porter, J.W. (1984): Pembina oilfield, in retrospect; *in* The Mesozoic of Middle North America, D.F. Stott and D.J. Glass (eds.), Canadian Society of Petroleum Geologists, Memoir 9, p. 1–13.
- Ogg, J.G., and Hinnov, L.A. (2012): Cretaceous; *in* The Geologic Time Scale 2012, Gradstein, F.M., Ogg, J.G., and Schmitz, M. (ed.), Elsevier Science & Technology (Vol. 2). Amsterdam, p. 793–853.
- Peachey, B. (2014): Mapping unconventional resource industry in the Cardium play region; New Paradigm Engineering Report prepared for PTAC Petroleum Technology Alliance Canada. May 1, 2014, 15 p.

- Pedersen, P.K., Fic, J.D. and Fraser, A. (2013): Integrated geological reservoir characterization of the Cardium light tight oil play, Pembina Field in Alberta; Unconventional Resources Technology Conference, p. 807–813.
- Pyrz, M.J. and Deutsch, C.V. (2014): Geostatistical reservoir modeling, 2<sup>nd</sup> Ed.; Oxford University Press, 433 p.
- Rutherford, R.L. (1927): Geology along the Bow River between Cochrane and Kananaskis, Alberta; Research Council of Alberta, Report 17, 64 p.
- Viau, C. and Nielsen K. (2010): Unconventional oil production in the Cardium Formation, East Pembina Area, Alberta, Canada; CSPG Core Conference, Calgary, Alberta, Canada, 4 p.
- Walker, J. D., Geiss, J. W., Bowring, S. A. and Babcock, L. E. (2012): Geologic Time Scale v. 4; Geological Society of America, <https://doi.org/10.1130/2012.CTS004R3C>.
- Walker, R.G., Plint, A.G., and Bergman, K.M. (1995): Biostratigraphic evaluation of sequence stratigraphic bounding surface: the Cardinal/Leyland unconformity ("E5/T5 surface") in the Cardium Formation (Upper Cretaceous; upper Turonian - lower Coniacian) at Seebe, Alberta: discussion; Bulletin of Canadian Petroleum Geology, v. 43, p. 343–346.
- Wiseman, A. C. (2014): Geologic framework, reservoir characterization and production analyses of the Cardium Formation: unconventionally developed North West Pembina Field, Alberta, Canada; M.Sc. thesis, University of Calgary, 296 p.